Characterization and generation of a standard-quantum-limit–beating catlike state through repetitive measurements

Mamiko Tatsuta,[1,*] Yuichiro Matsuzaki,[1,†] Hiroki Kuji,[1,2] Ryusuke Hamazaki,[3,4,‡] and Akira Shimizu[5,6]

[1]*Department of Electrical, Electronic, and Communication Engineering, Faculty of Science and Engineering, Chuo University, 1-13-27, Kasuga, Bunkyo-ku, Tokyo 112-8551, Japan*

[2]*Department of Physics, Tokyo University of Science, 1-3 Kagurazaka, Shinjuku, Tokyo 162-8601, Japan*

[3]*Nonequilibrium Quantum Statistical Mechanics RIKEN Hakubi Research Team, RIKEN Pioneering Research Institute, Wako, Saitama 351-0198, Japan*

[4]*RIKEN Center for Interdisciplinary Theoretical and Mathematical Sciences, RIKEN, Wako, Saitama 351-0198, Japan*

[5]*Institute for Photon Science and Technology, The University of Tokyo, 7-3-1 Hongo, Bunkyo-ku, Tokyo 113-0033, Japan*

[6]*Center for Quantum Information and Quantum Biology, The University of Osaka, Toyonaka, Osaka 560-0043, Japan*

(Received 12 August 2025; accepted 12 January 2026; published 10 February 2026)

Sensitivity in metrology without entanglement is limited by the standard quantum limit (SQL). Recent studies have found that the Heisenberg-limited scaling, the ultimate sensitivity in quantum metrology, can be achieved by generalized cat states, which are characterized by an index that indicates coherence among macroscopically distinct states and are associated with additive observables. Although generalized cat states include diverse states, encompassing classical mixtures of exponentially large numbers of states, the preparation of large generalized cat states has not been demonstrated yet. Here we characterize SQL-beating catlike states using the index q indicating macroscopic coherence and prove that any state with $q > 1.5$ has a potential to surpass the SQL when used as a sensor. We propose a protocol to generate them through repetitive measurements on a quantum spin system of N spins, which we call a spin ensemble. Starting from a thermal equilibrium state of the spin ensemble, we demonstrate that we can increase the coherence among the spin ensemble via repetitive weak measurements of its total magnetization, which is indirectly measured through an ancillary qubit collectively coupled to the ensemble. Notably, our method for creating the SQL-beating catlike states requires no dynamical control over the spin ensemble. As a potential experimental realization, we discuss a hybrid system composed of a superconducting flux qubit and donor spins in silicon. Our results pave the way for the realization of entanglement-enhanced quantum metrology in state-of-the-art technology.

DOI: 10.1103/ljb3-sdvb

I. INTRODUCTION

High-precision measurement is of paramount importance in both fundamental research and applied science [1–4]. Numerous critical parameters, including temperature, electric field, and pressure, require precise measurement. In particular, magnetic-field sensing has garnered considerable attention [5–7], serving not only to investigate material properties but also to elucidate biological mechanisms. Substantial efforts have been devoted to enhancing the sensitivity of magnetic-field sensors [8–25]. One promising approach to improving sensitivity is the utilization of qubits [26–34]. Magnetic fields induce shifts in the resonant frequency of qubits, allowing the estimation of magnetic-field strength via Ramsey-type measurements. When employing N qubits in separable states, the uncertainty (i.e., the reciprocal of sensitivity) scales as $N^{-1/2}$, which is called the standard quantum limit (SQL). Conversely, using a specific type of entangled state, the sensitivity scales as N^{-1}, achieving what is known as Heisenberg-limited scaling. In realistic scenarios, environmental decoherence cannot be avoided [9,11,19,22,23,25,35–40], making it challenging to reach Heisenberg-limited scaling. Nevertheless, it is established that under certain conditions of decoherence, it is possible to surpass the SQL in scaling. For instance, in the presence of time-inhomogeneous dephasing, the uncertainty scales as $N^{-3/4}$, referred to as the Zeno limit [9,19].

The concept of superposition involving macroscopically distinct states has been a topic of fundamental interest since its inception by Schrödinger [41]. The Greenberger-Horne-Zeilinger (GHZ) [42–44] state is a quintessential example of such a superposition. The GHZ state is expressed as $(|\uparrow\rangle^{\otimes N} + |\downarrow\rangle^{\otimes N})/\sqrt{2}$, where $|\uparrow\rangle$ and $|\downarrow\rangle$ are eigenstates of the Pauli operator $\hat{\sigma}_3$ with eigenvalues $+1$ and -1, respectively. Although a great deal of effort has been devoted to producing a superposition of macroscopically distinct states [45–56], a unified criterion to determine whether a given state contains such macroscopic superpositions remains elusive [57].

Among the various potential metrics, an index q [58], a real number satisfying $1 \leqslant q \leqslant 2$, is particularly noteworthy for gaining deeper insights into the correlation between cat states and sensor technologies. A state with $q = 2$ is referred to as a generalized cat state. Notably, there exists a generalized cat state $\hat{\rho}_m$ with exponentially small purity, i.e.,

*Contact author: mamikotatsuta@gmail.com
†Contact author: ymatsuzaki872@g.chuo-u.ac.jp
‡Contact author: ryusuke.hamazaki@riken.jp

$\mathrm{Tr}(\hat{\rho}_m^2) = \exp[-\Theta(N)]$ [59]. It has been shown that utilizing generalized cat states for magnetic-field sensing can achieve Heisenberg-limited scaling in the absence of decoherence [12] and the Zeno limit in the presence of time-inhomogeneous dephasing [9,19]. Thus, generalized cat states present a compelling metrological approach, leveraging quantum properties to significantly enhance sensitivity.

A theoretical proposal exists for the creation of a generalized cat state [60]. Starting with a thermal equilibrium state of a quantum spin system of N spins, which we call a spin ensemble, it is possible to generate the generalized cat state [60], by performing high-resolution, in this case $\Theta(1)$, measurement of magnetization. However, current technology does not allow such a high-resolution measurement of the magnetization of a spin ensemble. Consequently, a more accessible method for creating a large generalized cat state remains elusive.

In this study, we first use the index q to characterize states that are advantageous for quantum sensing, i.e., beating the SQL although less sensitive than generalized cat states. We call such states, which are shown to satisfy $1.5 < q < 2$, the SQL-beating catlike states. We then propose a method to create such SQL-beating states from a thermal equilibrium state of a spin ensemble through repetitive low-resolution measurements of the total magnetization, utilizing an ancillary qubit coupled with the spin ensemble. We prove that we obtain a SQL-beating catlike state with probability 1 in the large-N limit. We also perform numerical simulations to observe the gradual emergence of such a state.

This paper is outlined as follows. In Sec. II we review three important notions: the definition of the index q, a recipe to create a generalized cat state via single projective measurement, and the basics of quantum metrology. Section III discusses our finding on the relation between the sensitivity and the value of q, in particular when $1.5 < q < 2$. In Sec. IV we propose a protocol to create a SQL-beating catlike state via repetitive measurements, in particular within a spin ensemble in a solid-state system read out by a superconducting qubit. In Sec. V we analyze the final state of the spin ensemble after measurements and clarify the condition of successfully generating a generalized cat state. We also discuss the success probability and evaluate how many measurements are required to approximately obtain the state we want. Numerical simulations are given in Sec. VI, and we indeed observe the emergence of SQL-beating catlike states. Section VII summarizes the paper and provides an outlook for future work.

II. PRELIMINARIES

We first review the previous works on generalized cat states and a way of obtaining them from thermal equilibrium states through a single measurement. We also review Ramsey-type quantum metrology using highly entangled states. Throughout this paper, we take $\hbar = 1$.

A. Generalized cat states

First, let us briefly review the concept of generalized cat states, characterized by an index denoted by q [58]. For a comprehensive discussion, refer to Ref. [61].

The index q is utilized to detect macroscopic coherence in a given quantum state $\hat{\rho}$, which may be pure or mixed. It is defined through the relation

$$\max\left\{\max_{\hat{A}} \tfrac{1}{2}\|[\hat{A},[\hat{A},\hat{\rho}]]\|_1, N\right\} = \Theta(N^q), \tag{1}$$

where $\|\hat{X}\|_1 = \mathrm{Tr}\sqrt{\hat{X}^\dagger \hat{X}}$ is the trace norm and $\hat{A}$ is an additive observable, defined as $\hat{A} = \sum_{l=1}^{N} \hat{a}(l)$, with $\hat{a}(l)$ acting on a single spin at site l [62]. By definition, the index satisfies the condition of $1 \leqslant q \leqslant 2$. The trace norm can be expressed as

$$\tfrac{1}{2}\|[\hat{A},[\hat{A},\hat{\rho}]]\|_1 = \max_{\hat{\eta}} \mathrm{Tr}(\hat{\eta}[\hat{A},[\hat{A},\hat{\rho}]]) \tag{2}$$

$$= \max_{\hat{\eta}} \sum_{A,A',\nu,\nu'} (A-A')^2 \langle A,\nu|\hat{\rho}|A',\nu'\rangle \times \langle A',\nu'|\hat{\eta}|A,\nu\rangle, \tag{3}$$

where A ($|A,\nu\rangle$) are eigenvalues (eigenstates) of $\hat{A}$, i.e., $\hat{A}|A,\nu\rangle = A|A,\nu\rangle$, with ν labeling the degeneracy, and $\hat{\eta}$ is a projection operator, which satisfies $\hat{\eta}^2 = \hat{\eta}$. From this expression, we find that $\frac{1}{2}\|[\hat{A},[\hat{A},\hat{\rho}]]\|_1$ indicates macroscopic coherence between two macroscopically distinct states and that q can be interpreted as a measure to quantify how close the state is to the cat state. For example, it is evident that macroscopic coherence, i.e., $\langle A,\nu|\hat{\rho}|A',\nu'\rangle$ with $|A-A'| = \Theta(N)$ [or $(A-A')^2 = \Theta(N^2)$], has a substantial weight in the trace norm of the double commutator if the state has $q = 2$. Then we can conclude that a state $\hat{\rho}$ with $q = 2$ contains a substantial amount of superposition of macroscopically distinct states.

In addition to the index q, we introduce a term "a generalized cat state." We call $\hat{\rho}$ a generalized cat state of $\hat{A}$ if there exists a projection operator $\hat{\eta}$ such that

$$\mathrm{Tr}(\hat{\eta}[\hat{A},[\hat{A},\hat{\rho}]]) = \Theta(N^2) \tag{4}$$

for a given $\hat{A}$. From this definition, a generalized cat state has $q = 2$. Conversely, each state with $q = 2$ is regarded as a generalized cat state of some observable $\hat{A}$. As detailed in Sec. II C, the generalized cat state exhibits a significant advantage, i.e., beating the SQL, when used in metrology.

B. From a thermal equilibrium state to a generalized cat state

In this section we review a protocol to obtain a generalized cat state from a thermal equilibrium state of a spin ensemble using high-resolution measurements. We define $\hat{S}_\alpha = \sum_{i=1}^{N} \hat{\sigma}_\alpha(i)$, with $\alpha = x, y, z$, where $\hat{\sigma}_\alpha$ denotes a Pauli operator.

In [60] it was proven that a single ideal measurement of the total magnetization can transform a thermal equilibrium state into a generalized cat state. This protocol involves the following steps.

(i) Prepare the spins in a thermal equilibrium state in a magnetic field along the z axis, represented by h, at a temperature $1/\beta$. The Hamiltonian is $\hat{H}_\mathrm{P} = -\omega_\mathrm{P}\hat{S}_z$, where $\omega_\mathrm{P} = h$. The initial state is then given by $\hat{\rho}_\mathrm{P} = e^{\beta\omega_\mathrm{P}\hat{S}_z}/Z_\mathrm{P}$, where $Z_\mathrm{P} = \mathrm{Tr}(e^{\beta\omega_\mathrm{P}\hat{S}_z})$. Here the subscript P stands for the phosphorus donor electrons, which we consider as a spin ensemble to generate generalized cat states in Sec. IV A.

(ii) Perform a projection measurement onto the $\hat{S}_x = M$ subspace. The postmeasurement state is expressed as

$\hat{\rho}_{\rm PM} = \hat{\mathcal{P}}(M)e^{\beta\omega_{\rm P}\hat{S}_z}\hat{\mathcal{P}}(M)/Z_{\rm PM}$, where $\hat{\mathcal{P}}(M)$ denotes the projection onto the $\hat{S}_x = M$ subspace and $Z_{\rm PM} = {\rm Tr}[\hat{\mathcal{P}}(M)e^{\beta\omega_{\rm P}\hat{S}_z}]$.

It can be shown that

$$\mathrm{Tr}\{\hat{\mathcal{P}}(M)[\![\hat{S}_z,[\hat{S}_z,\hat{\rho}_{\rm PM}]]\!]\} = (N^2 - M^2)\tanh^2(\beta\omega_{\rm P}) + 2N, \tag{5}$$

indicating that $\hat{\rho}_{\rm PM}$ is a generalized cat state of $\hat{S}_z$ when $\beta\omega_{\rm P} = \Theta(N^0) > 0$ and $M \neq \pm N + o(N)$. Note that this value may be smaller than $\frac{1}{2}\|[\![\hat{S}_z,[\hat{S}_z,\hat{\rho}_{\rm PM}]]\!]\|_1$, since taking the trace norm $\|\hat{X}\|_1$ of the Hermitian $\hat{X}$ corresponds to applying a projection operator $\hat{\eta}_M$ that maximizes $2\,\mathrm{Tr}(\hat{\eta}_M\hat{X})$. Interestingly, for finite temperature $1/\beta$, this generalized cat state exhibits an exponentially small purity, i.e., $\mathrm{Tr}(\hat{\rho}_{\rm PM}^2) \leqslant \exp[-\Theta(N)]$, due to the highly mixed nature of the premeasurement Gibbs state. This explanation pertains to a simple case with no interactions between spins. However, it was also proven in [60] that a generalized cat state of $\hat{S}_z$ can be obtained even in the presence of interaction between the spins.

A significant challenge of this scheme lies in the requirement for high-resolution measurements. If the precision of the projection $\hat{\mathcal{P}}(M)$, equivalent to the minimum resolvable number of spins, is $\Theta(\sqrt{N})$, the conversion to a generalized cat state occurs with a probability of $\exp[-\Theta(N)]$. To achieve a generalized cat state with a probability that remains constant as N increases, the projection $\hat{\mathcal{P}}(M)$ must be performed with a precision of $\Theta(1)$. This level of precision is experimentally demanding with a single readout. In this paper we propose to overcome this difficulty by introducing repetitive measurements.

C. Ramsey-type quantum metrology

Next let us briefly review Ramsey-type quantum metrology [4] and elucidate how we can utilize our highly entangled state. We adopt this as the basic strategy in our protocol. Assume that the Hamiltonian describing the interaction with the magnetic field is $\hat{H} = -\omega\hat{S}_z$. In a Ramsey-type measurement protocol, a sensor state $\hat{\rho}$ is exposed to the target field for a time $t_{\rm int}$, resulting in the state evolution

$$\hat{\rho}(t_{\rm int}) = e^{i\omega t_{\rm int}\hat{S}_z}\hat{\rho}e^{-i\omega t_{\rm int}\hat{S}_z}. \tag{6}$$

Then a projective measurement is performed. This projection operator can be chosen to optimize the sensitivity. The probability P of the projection $\hat{\eta}$ is given by

$$P = \mathrm{Tr}[\hat{\eta}\hat{\rho}(t_{\rm int})]. \tag{7}$$

This protocol is repeated $T/t_{\rm int} \gg 1$ times, where T is the total measurement time. Here we assume that the state preparation and readout times are negligible compared to $t_{\rm int}$. From the measurement outcomes, the parameter ω can be estimated with an uncertainty [12]

$$\delta\omega = \frac{\sqrt{P(1-P)}}{\left|\frac{dP}{d\omega}\right|}\frac{1}{\sqrt{T/t_{\rm int}}}. \tag{8}$$

The inverse of the uncertainty defines the sensitivity. If the initial state is separable (for which $q = 1$), then

$$\delta\omega = \Theta(N^{-1/2}), \tag{9}$$

which is known as the standard quantum limit. Conversely, a state with $q = 2$ provides us with

$$\delta\omega = \Theta(N^{-1}), \tag{10}$$

which is referred to as the Heisenberg-limited scaling [12]. This enhancement of sensitivity in scaling is crucial in quantum metrology.

The generalized cat state of $\hat{A}$ can be employed to estimate a parameter ω coupled to $\hat{A}$, where the state evolves under an interaction Hamiltonian $\hat{H} = \omega\hat{A}$. It has been demonstrated that the target parameter ω in this setup can be estimated at the ultimate scaling sensitivity: the Heisenberg-limited scaling $\delta\omega = \Theta(N^{-1})$ in the absence of noise and the Zeno limit $\delta\omega = \Theta(N^{-3/4})$ in the presence of time-inhomogeneous dephasing [61]. Additionally, the method in [61] provides a detailed prescription of how to achieve this sensitivity using the generalized cat states. More specifically, the Ramsey-type protocol is utilized, where the generalized cat state is prepared as a probe state, exposed to the target field, and subsequently measured by the projection $\hat{\eta}$.

It is important to note that the quantum Fisher information offers the highest sensitivity attainable with a given state via the Cramér-Rao bound [8], assuming an optimal positive-operator-valued measure (POVM) is chosen. However, finding the optimal POVM is a core mission in quantum metrology [63] and its physical implementation may be nontrivial. In contrast, the approach using the generalized cat state as proposed in [61] is advantageous because it demonstrates practical experimental implementation. Furthermore, we introduce here a feasible procedure to obtain states with high-q value and explore their features both analytically and numerically.

In the following section we discuss a relation between index q and sensitivity, generalizing the above relations.

III. SQL-BEATING CATLIKE STATES

Given the preliminaries discussed above, we now show our first important result that states with $q > 1.5$ can serve as sensors surpassing the SQL. Specifically, we show that

$$\delta\omega \leqslant 1/\Theta(N^{q-1}), \tag{11}$$

that is, the sensitivity beyond the SQL is achievable for $q > 1.5$.

Let $\hat{\eta}$ be the projection operator that satisfies the following:

$$\tfrac{1}{2}\|[\hat{S}_z,\hat{\rho}]\|_1 = \mathrm{Tr}(\hat{\eta}[\hat{S}_z,\hat{\rho}]). \tag{12}$$

We then obtain the inequality

$$\tfrac{1}{2}\|[\![\hat{S}_z,[\hat{S}_z,\hat{\rho}]]\!]\|_1 \leqslant 2N\tfrac{1}{2}\|[\hat{S}_z,\hat{\rho}]\|_1 = 2N|\mathrm{Tr}(\hat{\eta}[\hat{S}_z,\hat{\rho}])|. \tag{13}$$

This inequality implies that if $\hat{\rho}$ is a generalized cat state of $\hat{S}_z$, then $\|[\hat{S}_z,\hat{\rho}]\|_1 = \Theta(N)$.

Using the Baker-Hausdorff formula, we have

$$\hat{\rho}(t) = \sum_{k=0}^{\infty}\frac{(i\omega t)^k}{k!}[\hat{S}_z,\hat{\rho}]_k, \tag{14}$$

where we define $[\hat{S}_z,\hat{\rho}]_0 = \hat{\rho}$ and $[\hat{S}_z,\hat{\rho}]_k = [\![\hat{S}_z,[\hat{S}_z,\hat{\rho}]_{k-1}]\!]$.

Hence, we have

$$\left|\frac{dP}{d\omega}\right| = \left|\mathrm{Tr}\left(\hat{\eta}\sum_{k=1}^{\infty}\frac{-it_{\mathrm{int}}(i\omega t_{\mathrm{int}})^{k-1}}{(k-1)!}[\hat{S}_z,\hat{\rho}]_k\right)\right| \tag{15}$$

$$\simeq |\mathrm{Tr}\{\hat{\eta}(-it_{\mathrm{int}})[\hat{S}_z,\hat{\rho}]\}| \quad (\omega t_{\mathrm{int}} N \ll 1) \tag{16}$$

$$= t_{\mathrm{int}}|\mathrm{Tr}(\hat{\eta}[\hat{S}_z,\hat{\rho}])|, \tag{17}$$

where we have used $\omega t_{\mathrm{int}} N \ll 1$, which is a common assumption in quantum metrology.

Therefore, we obtain the inequality that ensures the advantage of states with $q > 1.5$,

$$\delta\omega \simeq \frac{\sqrt{P(1-P)}}{|t_{\mathrm{int}}\mathrm{Tr}(\hat{\eta}[\hat{S}_z,\hat{\rho}])|}\frac{1}{\sqrt{T/t_{\mathrm{int}}}} \tag{18}$$

$$\leqslant \frac{1/2}{\frac{1}{2}\|[\hat{S}_z,\hat{\rho}]\|_1}\frac{1}{\sqrt{Tt_{\mathrm{int}}}} \tag{19}$$

$$\leqslant \frac{N}{\frac{1}{2}\|[\hat{S}_z,[\hat{S}_z,\hat{\rho}]]\|_1}\frac{1}{\sqrt{Tt_{\mathrm{int}}}} \tag{20}$$

$$= \frac{1}{\Theta(N^{q-1})}\frac{1}{\sqrt{Tt_{\mathrm{int}}}}, \tag{21}$$

which gives (11).

This bound is loose when considering separable states, as they provide a scaling of $\delta\omega = \Theta(N^{-1/2})$, while this bound gives $\delta\omega \leqslant \Theta(N^0)$. However, this bound is significant for states with $q > 1.5$, because they surpass the SQL in scaling. Therefore, not only the states with $q = 2$ but also states with $1.5 < q < 2$ are advantageous for quantum metrology. We refer to such states as SQL-beating catlike states and illustrate their emergence as the result of repetitive measurements.

Note that the inequality (18) provides us with the upper bound of $\delta\omega$, while the Cramér-Rao bound provides the lower bound. More specifically, the actual value of uncertainty might be better than what we calculate through our inequality, while the Cramér-Rao bound indicates the lowest limit that might be difficult to achieve because of the imperfection of a realistic setup.

IV. SETUP OF EMERGENCE OF SQL-BEATING CATLIKE STATES VIA REPETITIVE MEASUREMENTS

We present our protocol for generating SQL-beating catlike states through repetitive measurements. The procedure involves coupling a spin ensemble with an ancillary qubit and subsequently reading out the total magnetization of the spins via the projective measurement of the ancillary qubit. Given that a single measurement of the ancillary qubit yields a binary result, it does not provide direct information on the total magnetization of the spins. However, we demonstrate that through repeated measurements, the thermal equilibrium state is converted into SQL-beating catlike states due to measurement backaction. Although this scheme can be implemented in various physical systems, we primarily focus on a hybrid system consisting of an electron spin ensemble and a superconducting flux qubit (FQ), which often plays a key role in quantum computing. Our approach aims to generate generalized cat states within the electron spin ensembles by measuring the spin magnetization with the FQ. In the following, we briefly review each system and subsequently propose our scheme.

A. Spin ensemble

First, we introduce a spin ensemble that we convert into generalized cat states. Specifically, we consider phosphorus (P) donor electrons in a pure ^{28}Si substrate [64]. We assume that the temperature is low so that all donor electrons are trapped by the donors. The P donor electron possesses a spin of 1/2. The donors are distributed randomly in the substrate, and we assume that the donor density is low, typically 10^{15} cm^{-3} [64], so that spin-spin interactions are negligible. Notably, these spins exhibit a long coherence time of around 10 s [64], making them ideal for the creation and manipulation of superposition of macroscopically distinct states.

By applying a magnetic field h along the z axis, the two energy levels are split by the Zeeman energy. The Hamiltonian is described as

$$\hat{H}_{\mathrm{P}} = -\omega_{\mathrm{P}}\sum_{j=1}^{N}\hat{\sigma}_z(j) =: -\omega_{\mathrm{P}}\hat{S}_z, \tag{22}$$

where $\omega_{\mathrm{P}} = h$. This ω_{P} is $\Theta(1)$ and known, unlike the target parameter ω in Sec. II C. The spin ensemble is initially prepared in the canonical Gibbs state with the inverse temperature β [65],

$$\hat{\rho}_{\mathrm{P}}(0) = e^{-\beta\hat{H}_{\mathrm{P}}}/\mathrm{Tr}(e^{-\beta\hat{H}_{\mathrm{P}}}), \tag{23}$$

which has the total spin $\langle\hat{S}_z\rangle = \Theta(N)$ parallel to h. We will manipulate this state by measuring $\hat{S}_x$, the total spin component perpendicular to h, with the superconducting flux qubit, which we review in the following section.

B. Superconducting flux qubit

A superconducting FQ is an artificial two-level system [66–69], often used in quantum computing. The FQ comprises a superconducting loop with several (typically three) Josephson junctions, operating at temperatures in the tens of millikelvin. Within the loop, a persistent current I_q flows either clockwise or counterclockwise. The clockwise current corresponds to a state $|R\rangle$, while the counterclockwise current corresponds to the state $|L\rangle$. By defining $\hat{\Sigma}_3 := |R\rangle\langle R| - |L\rangle\langle L|$ and $\hat{\Sigma}_1 := |R\rangle\langle L| + |L\rangle\langle R|$, the Hamiltonian of the FQ can be expressed as

$$\hat{H}_{\mathrm{FQ}} = \epsilon\hat{\Sigma}_3 + \Delta\hat{\Sigma}_1 \simeq \epsilon\hat{\Sigma}_3, \tag{24}$$

where $\epsilon = 2I_q(\Phi - \Phi_0/2)$ is an energy bias, with Φ representing the magnetic flux penetrating the loop of the FQ and Φ_0 denoting a flux quantum. Also, Δ is the tunneling energy, and we assume $\Delta \ll \epsilon$. Although Δ is small, it controls the persistent current of the flux qubit [70–72] and will therefore play a crucial role in our scheme. We will take its effect into account whenever necessary, while otherwise we approximate $\hat{H}_{\mathrm{FQ}}$ as $\epsilon\hat{\Sigma}_3$.

A flux qubit can be utilized as a sensitive magnetometer for detecting the penetrating magnetic flux Φ [22,29,30,73,74]. To estimate ϵ, which directly translates to estimating the external flux Φ, the following procedure is employed. First, the

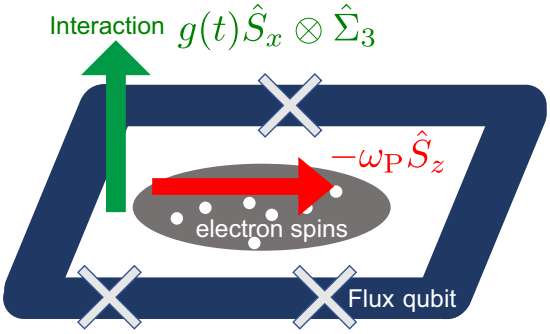

FIG. 1. Schematic of the spin ensemble and the FQ. The electron spins (white dots) are situated on the substrate (gray oval), which is placed within the loop of the FQ (navy parallelogram). An external magnetic field (red arrow) is applied along the z axis to induce the Zeeman energy $-\omega_P \hat{S}_z$. The interaction between the spin ensemble and the FQ is represented by a green arrow.

flux qubit is prepared in the state

$$|+\rangle := (|R\rangle + |L\rangle)/\sqrt{2}. \tag{25}$$

This state can be prepared by applying a $\pi/2$ pulse of a resonant microwave [75], a step referred to as initialization. By exposing this state to the target external magnetic field corresponding to ϵ for a duration t, we obtain $(e^{-i\epsilon t}|R\rangle + |L\rangle)/\sqrt{2}$. For readout, we perform a single-qubit rotation using a microwave pulse, followed by measurement using a Josephson bifurcation amplifier [76,77] or a dispersive readout with a Josephson parametric amplifier. This process corresponds to a projective measurement in the $\hat{\Sigma}_2 := i|L\rangle\langle R| - i|R\rangle\langle L|$ basis.

Each measurement yields either $+1$ or -1 from the readout apparatus of the FQ, with a probability $P = \cos^2(\epsilon t/2)$ for $+1$ and $1 - P = \sin^2(\epsilon t/2)$ for (-1). By repeating this procedure, we can accurately estimate P, thereby reducing the uncertainty in the estimation of ϵ. According to the central-limit theorem, the uncertainty $\delta\epsilon$ depends on the square root of the number of repetitions m:

$$\delta\epsilon \propto \frac{1}{\sqrt{m}}. \tag{26}$$

In this paper we increase the m repetitive measurements with a FQ to convert a thermal equilibrium state into a generalized cat state.

C. Hybrid system

We now introduce the hybrid system comprising N electron spins and a FQ [78–82], where the FQ serves as an ancillary qubit to repetitively measure the total magnetization of the spin ensemble.

As illustrated in Fig. 1, an ensemble of donor electron spins in silicon is placed inside the loop of the FQ. We apply a magnetic field parallel to the plane of the FQ loop corresponding to the application of $\omega_P \hat{S}_z$ as described in Sec. II B. We assume that the spin ensemble's x axis is orthogonal to the plane of the loop. The FQ has two basis states corresponding to the clockwise and counterclockwise currents. These currents generate magnetic fields that shift the Zeeman energy of the electron spin in the x direction. This state-dependent energy shift induces a magnetic interaction between electron spins and the FQ, described by the interaction Hamiltonian

$$\hat{H}_{\rm int} = g(t)\hat{S}_x \otimes \hat{\Sigma}_3, \tag{27}$$

where $g(t)$ denotes the coupling strength between them.

The total Hamiltonian of the system is

$$\hat{H} = \hat{H}_{\rm FQ} + \hat{H}_P + \hat{H}_{\rm int}. \tag{28}$$

If the interaction induces a frequency shift on the FQ, we can use the FQ to detect the magnetization of the spin ensemble by performing the Ramsey-type measurements on the FQ. We take $h = \omega_P$ large enough such that

$$|g(t)| \ll \omega_P \tag{29}$$

is satisfied. Under this condition, a dc (time-independent) term in $g(t)$ is unimportant because it will be dropped due to a rotating-wave approximation. By contrast, an ac (time-dependent) term in $g(t)$ can induce significant resonant effects if its frequency is approximately equal to ω_P. Therefore, we consider the time-dependent coupling

$$g(t) = g\cos(2\omega_P t) = g\frac{e^{2i\omega_P t} + e^{-2i\omega_P t}}{2}. \tag{30}$$

We can achieve such modulation of the coupling strength by altering the tunneling energy Δ of the FQ since the persistent current of the FQ depends on the tunneling energy [72]. Alternatively, with a time-independent coupling strength, we could perform many π pulses on the FQ sequentially, akin to dynamical decoupling [75], causing the effective coupling strength to oscillate temporarily. In this paper, we focus on the former strategy.

Because of Eqs. (29) and (30), the rotating-wave approximation works well. In the rotating frame defined by $\hat{V} = \exp(-i\omega_P t\hat{S}_z + i\epsilon\hat{\Sigma}_3 t)$, we have

$$\hat{H}_R = \hat{V}\hat{H}\hat{V}^\dagger - i\hat{V}\frac{d\hat{V}^\dagger}{dt} \tag{31}$$

$$= g(t)\frac{\hat{S}_+ e^{-2i\omega_P t} + \hat{S}_- e^{2i\omega_P t}}{2} \otimes \hat{\Sigma}_3, \tag{32}$$

where we use $\hat{S}_x = (\hat{S}_+ + \hat{S}_-)/2$. Thus, the Hamiltonian in the rotating frame becomes

$$\hat{H}_R \simeq \frac{g}{2}\hat{S}_x \otimes \hat{\Sigma}_3. \tag{33}$$

This Hamiltonian indicates that the spin magnetization along the x axis induces a frequency shift on the FQ, allowing us to use Ramsey measurements on the FQ to detect the spin ensembles. Importantly, in this scenario, we do not need to control the spin ensemble with microwave pulses.

As depicted in Fig. 2, we assume that $g(t) = 0$ during the initialization and readout of the FQ, whereas it oscillates as Eq. (30) during interaction. Even if the coupling strength has a dc component, we can ignore its effect, as mentioned above. Below we analyze how the state of the spin ensemble changes by repeating these Ramsey measurements.

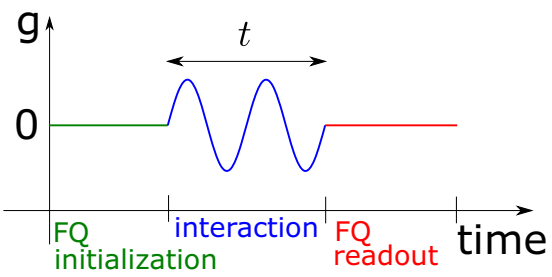

FIG. 2. Schematic of the time dependence of $g(t)$. To induce an interaction between the FQ and the spin ensemble, we modulate the coupling strength to oscillate.

V. ENTANGLEMENT GENERATION BETWEEN ELECTRON SPINS VIA REPETITIVE MEASUREMENTS WITH THE FQ

In this section we show our second main result that the SQL-beating states are generated under the evolution of the spin ensemble's state through a sequence of Ramsey-type measurements involving the FQ. With the ground state at temperature zero as the initial state of the spin ensemble, we obtain a certain Dicke state after infinitely many readout processes in a reasonable parameter regime. We see that the probability of obtaining a generalized cat state as a final state is asymptotically 1 for large N.

A. State after m measurements

In this section we consider what state we get after m measurements are applied to the spin ensemble. Let $\hat{\rho}_{\rm P}(m)$ denote the density matrix of the spin ensemble after the mth measurement by the FQ, where $\hat{\rho}_{\rm P}(0)$ is given by Eq. (23). By performing the $(m+1)$th measurement on $\hat{\rho}_{\rm P}(m)$, we obtain either of

$$\hat{\rho}_{\rm P}(m+1) = \frac{\hat{W}_+\hat{\rho}_{\rm P}(m)\hat{W}_+^\dagger}{\mathrm{Prob}(\Sigma_2=+1)}, \tag{34}$$

$$\hat{\rho}_{\rm P}(m+1) = \frac{\hat{W}_-\hat{\rho}_{\rm P}(m)\hat{W}_-^\dagger}{\mathrm{Prob}(\Sigma_2=-1)}, \tag{35}$$

depending on the measurement results, where

$$\hat{W}_+ := \langle +_y|e^{-i(g/2)\hat{S}_x\otimes\hat{\Sigma}_3 t}|+\rangle = \frac{1-i}{\sqrt{2}}\sin\left(\frac{\pi}{4}+\frac{gt\hat{S}_x}{2}\right), \tag{36}$$

$$\hat{W}_- := \langle -_y|e^{-i(g/2)\hat{S}_x\otimes\hat{\Sigma}_3 t}|+\rangle = \frac{1+i}{\sqrt{2}}\sin\left(\frac{\pi}{4}-\frac{gt\hat{S}_x}{2}\right) \tag{37}$$

are measurement operators. For a detailed derivation, see Appendix A. Here $|\pm_y\rangle$ denotes the eigenvectors of $\hat{\Sigma}_2$ with an eigenvalue of ±1. The probability for the corresponding projection is given by

$$\mathrm{Prob}(\Sigma_2=\pm1) = \mathrm{Tr}[\hat{W}_\pm\hat{\rho}_{\rm P}(m)\hat{W}_\pm^\dagger]. \tag{38}$$

To elucidate the effect of repetitive measurements, we study the zero-temperature limit $\beta\to\infty$ in this section and leave the study of the case of finite temperature to the next section. In the zero-temperature limit, the initial state of the spin ensemble is a pure state $|\uparrow\rangle^{\otimes N}$. Hence we analyze $|\phi_m\rangle$, a pure state after m measurements. At each readout process, either $\hat{W}_+$ or $\hat{W}_-$ is probabilistically applied to the state of the spin ensemble. This means there are 2^m possible trajectories when m measurements are performed by the FQ. Fortunately, since $\hat{W}_+$ commutes with $\hat{W}_-$, the number of effective trajectories is reduced and there are only $m+1$ distinct trajectories to consider. Let k denote the number of times $\hat{W}_+$ is applied to the state during the m measurements. For a given k, the final state can be expressed as

$$|\phi_m\rangle = (\hat{W}_+)^k(\hat{W}_-)^{m-k}|\uparrow\rangle^{\otimes N}/\mathrm{norm}, \tag{39}$$

where

$$(\mathrm{norm})^2 = \langle\uparrow|^{\otimes N}(\hat{W}_+^\dagger\hat{W}_+)^k(\hat{W}_-^\dagger\hat{W}_-)^{m-k}|\uparrow\rangle^{\otimes N}. \tag{40}$$

Assuming

$$gtN < \pi/2 \tag{41}$$

for simplicity for a while, we can prove that for $m\gg1$, $(\hat{W}_+)^k(\hat{W}_-)^{m-k}$ attains the eigenvalue with the largest modulus for eigenstates of $\hat{S}_x$, when the corresponding eigenvalue S_x becomes the closest to $(gt)^{-1}\arcsin(2k/m-1)$. Details are provided in Appendix B.

Importantly, it is known that if an operator $\hat{K}$ is applied infinitely many times to the system, the system converges to the eigenstate of $\hat{K}$ corresponding to the eigenvalue with the largest modulus, provided it is unique [83–85]. Furthermore, in our case, we obtain $(\hat{W}_+)^k(\hat{W}_-)^{m-k} = [(\hat{W}_+)^\alpha(\hat{W}_-)^{(1-\alpha)}]^m$ for $k=\alpha m$, where $0\leqslant\alpha\leqslant1$. It is worth mentioning that $\hat{K} = (\hat{W}_+)^\alpha(\hat{W}_-)^{(1-\alpha)}$ and $(\hat{W}_+)^k(\hat{W}_-)^{m-k}$ take the largest eigenvalue with the same eigenstate. By applying this fact to our case, we obtain

$$|\phi_m\rangle \simeq \left|S_x = (gt)^{-1}\arcsin\left(\frac{2k}{m}-1\right)\right\rangle \tag{42}$$

for large m, if we assume that $(gt)^{-1}\arcsin(\frac{2k}{m}-1)$ is an integer. Here we define

$$|S_x=\theta\rangle := \left|D_N^{(\theta)}\right\rangle, \tag{43}$$

where $|D_N^{(\theta)}\rangle$ is a Dicke state given by

$$\left|D_N^{(\theta)}\right\rangle = \sqrt{\binom{N}{\frac{N+\theta}{2}}^{-1}}\sum_{\sigma\in\mathcal{S}_N}\mathcal{P}_\sigma(|+\rangle^{\otimes(N+\theta)/2}|-\rangle^{\otimes(N-\theta)/2}), \tag{44}$$

with $\mathcal{P}_\sigma$ denoting the permutation of spins and the summation taken over all different permutations in the permutation group $\mathcal{S}_N$ [86–88].

For an illustration, consider the example where $k=m/2$ for an even number m. An operator $\hat{W}_+\hat{W}_- = \cos(gt\hat{S}_x)/2$ is applied $m/2$ times. In the region $-\pi/2 < x < \pi/2$, the function $\cos(x)$ attains its maximum value of 1 at $x=0$. Therefore, we obtain

$$|\phi_m\rangle \to |S_x=0\rangle \tag{45}$$

in the limit of $m\to\infty$.

Note that S_x takes only integer values, while $(gt)^{-1}\arcsin(\frac{2k}{m}-1)$ is not necessarily an integer. This

necessitates refining the formula (42) as follows. In the limit of $m \to \infty$, the final state converges to

$$\lim_{m\to\infty} |\phi_m\rangle = |S_x = L\rangle, \tag{46}$$

where L is the integer closest to $(gt)^{-1}\arcsin(2k/m-1)$. If $(gt)^{-1}\arcsin(2k/m-1)$ is a half-integer, there are two possible states with eigenvalues whose modulus is the largest. In this case, the final state depends on the initial state's weight about these two states. This idea can be applied also in the next paragraph.

In actual experiments, it is not always possible to satisfy the condition of $gtN < \pi/2$. In a region $gtN \geqslant \pi/2$, the operator $(\hat{W}_+)^k(\hat{W}_-)^{m-k}$ takes the eigenvalue with the largest modulus when S_x takes either of the following values:

$$\theta_1(n) := \left[\arcsin\left(\frac{2k}{m}-1\right)+2n\pi\right]\Big/gt, \tag{47}$$

$$\theta_2(n') := \left[\pi-\arcsin\left(\frac{2k}{m}-1\right)+2n'\pi\right]\Big/gt. \tag{48}$$

Here n and n' are integers that satisfy

$$-gtN \leqslant \arcsin\left(\frac{2k}{m}-1\right)+2n\pi \leqslant gtN, \tag{49}$$

$$-gtN \leqslant \pi-\arcsin\left(\frac{2k}{m}-1\right)+2n'\pi \leqslant gtN, \tag{50}$$

where we use $-N \leqslant S_x \leqslant N$. As we have discussed in the preceding paragraph, the final state should be $|S_x = L\rangle$, where L is the integer closest to the largest (in magnitude) eigenvalue of $(\hat{W}_+)^k(\hat{W}_-)^{m-k}$, among $\theta_1(n)$ and $\theta_2(n')$ with multiple candidates of n and n' (we assume that such L is unique for simplicity). This implies that the integer L is taken as

$$L = \begin{cases} \theta_1(n), & \min_{n\in\mathbb{Z}} h_1(n) \leqslant \min_{n'\in\mathbb{Z}} h_2(n') \\ \theta_2(n'), & \min_{n\in\mathbb{Z}} h_1(n) > \min_{n'\in\mathbb{Z}} h_2(n'), \end{cases} \tag{51}$$

where

$$h_1(n) := |\theta_1(n) - \mathrm{round}[\theta_1(n)]|, \tag{52}$$

$$h_2(n') := |\theta_2(n) - \mathrm{round}[\theta_2(n)]|. \tag{53}$$

Here $\mathrm{round}(x)$ is the integer closest to x.

B. Variance of $\hat{S}_z$ in $\hat{\rho}_{\mathrm{P}}(m)$

Next we examine whether these postmeasurement states are generalized cat states. As we have clarified in the preceding section, the final state, i.e., $\hat{\rho}_{\mathrm{P}}(m)$ with $m \to \infty$, is a pure state when the initial state is a pure state $|\uparrow\rangle^{\otimes N}$. If the variance of an additive observable is of the order of N^2, such a pure state is a generalized cat state [58,61].

Calculating the variance of $\hat{S}_z$ for $|S_x = \xi\rangle$, we obtain

$$\begin{aligned}&\langle S_x=\xi|\hat{S}_z^2|S_x=\xi\rangle - \langle S_x=\xi|\hat{S}_z|S_x=\xi\rangle^2 \\ &\quad = \frac{N^2-\xi^2}{2}+N.\end{aligned} \tag{54}$$

This shows that, as long as there exists a positive N-independent constant δ (<1) such that $|\xi/N| < 1-\delta$ is satisfied, $|S_x = \xi\rangle$ is a generalized cat state. In the case $gtN < \pi/2$, the final state $|S_x \simeq (gt)^{-1}\arcsin[(2k-m)/m]\rangle$ is a generalized cat state if there exists a positive constant δ' (<1) such that $|(Ngt)^{-1}\arcsin[(2k-m)/m]| < 1-\delta'$ is satisfied, assuming for simplicity that L in the preceding section is uniquely determined. Intuitively, this can be explained as follows: Generalized cat states are produced by the m measurements when k is far enough from 0 and m so that $(gt)^{-1}\arcsin[(2k-m)/m]$ is not as large as N.

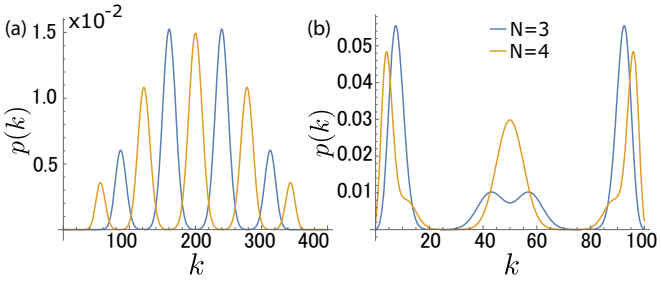

FIG. 3. Plot of the probability $p(k)$ of obtaining the trajectories in which $\hat{W}_+$ is applied k times, as described in Eq. (56), against k. In (a) the parameters are $gt = 0.2$, $m = 400$, and $N = 3$ (blue) and $N = 4$ (yellow), satisfying $gtN < \pi/2$. In this case, $p(k)$ is approximately given by the sum of the sharp normal-distribution-like peaks, whose heights become larger when they are closer to $k = m/2$. In (b) the parameters are $gt = 1.0$, $m = 100$, and $N = 3$ (blue) and $N = 4$ (yellow), satisfying $gtN \geqslant \pi/2$.

C. Probability of trajectories

We investigate the success probability of creating a generalized cat state when the initial state is $|\uparrow\rangle^{\otimes N}$.

Let $p(k)$ denote the probability of obtaining the trajectories in which $\hat{W}_+$ is applied k times. Since there are $\binom{m}{k}$ trajectories for a given k, the probability $p(k)$ is calculated as (see Appendix C for derivation)

$$p(k) = \binom{m}{k}\langle\uparrow|^{\otimes N}(\hat{W}_+^\dagger\hat{W}_+)^k(\hat{W}_-^\dagger\hat{W}_-)^{m-k}|\uparrow\rangle^{\otimes N} \tag{55}$$

$$\begin{aligned}&= \binom{m}{k}\frac{1}{2^N}\sum_{r=0}^{N}\binom{N}{r} \\ &\quad\times\left(\frac{1+\sin[gt(2r-N)]}{2}\right)^k \\ &\quad\times\left(\frac{1-\sin[gt(2r-N)]}{2}\right)^{m-k}.\end{aligned} \tag{56}$$

This $p(k)$ exhibits markedly different behaviors for various parameters (Fig. 3). For $gtN < \pi/2$, there are two highest peaks near $k = m/2$ for odd N, whereas there is a single highest peak at $k = m/2$ for even N. Additionally, the probabilities $p(0)$ and $p(m)$ are small.

Notably, we can prove that the success probability of generating a generalized cat state is sufficiently large. In particular, we can show that the probability approaches 1 as

$$\lim_{N\to\infty}\lim_{m\to\infty}{\sum_k}' p(k) = 1 \quad \text{when } gtN < \pi/2, \tag{57}$$

where $\sum_k'$ denotes the sum taken over k such that the corresponding stationary states are the generalized cat states. In

fact, in the limit $m \to \infty$, $p(k)$ can be regarded as a sum of the sharp normal-distribution peaks [as in Fig. 3(a)]. Then taking $N \to \infty$ leads to the concentration of the peaks towards $k \simeq m/2$, resulting in $\sum_k' p(k) \to 1$. For the detailed proof, see Appendix D. This is intuitive because we obtain a generalized cat state unless k is close to 0 or m when $gtN < \pi/2$, which is unlikely, as already speculated from Fig. 3(a).

For $gtN \geqslant \pi/2$, $p(k)$ exhibits a different behavior [see Fig. 3(b)]. We observe that $p(0)$ and $p(m)$ have relatively large values. However, we still obtain generalized cat states with a reasonable success probability, as we numerically find in the next section.

D. Required number of measurements

As explained in Sec. V A, an infinite number of measurements convert the initial state to $|S_x = L\rangle$. In this section we discuss how many measurements are required to approximately obtain this stationary state, assuming the case $gtN < \pi/2$.

For this purpose, we evaluate the spectral gap characterizing the dynamics. More precisely, we consider the spectrum $\{\lambda_a\}$ $(\lambda_1 \leqslant \lambda_2 \leqslant \cdots)$ of an operator

$$-\frac{1}{2m}\ln(\hat{W}_+^k\hat{W}_-^{m-k})(\hat{W}_+^k\hat{W}_-^{m-k})^\dagger = -\frac{1}{2}\ln\hat{K}\hat{K}^\dagger, \tag{58}$$

with $\hat{K} = \hat{K}^\dagger = (\hat{W}_+)^\alpha(\hat{W}_-)^{1-\alpha}$ and $\alpha = k/m$, which is called the Lyapunov spectrum of a trajectory under measurement [89,90]. The inverse of the gap of the Lyapunov spectrum, $\lambda_2 - \lambda_1$, is known to provide the timescale for relaxation to the final state. This is because the ratio of weights between the longest-lived decaying mode and the final state is evaluated by $e^{-\lambda_2 m}/e^{-\lambda_1 m}$, which becomes approximately e^{-1} when $m \simeq m_{\rm relax} := (\lambda_2 - \lambda_1)^{-1}$.

Since $\hat{W}_\pm$ are diagonal in the $\hat{S}_x$ basis, the above operator is simply given by $-\ln f(gt\hat{S}_x)$,

$$-\ln f(gt\hat{S}_x),$$

where $f(x) := \sin^\alpha(\frac{\pi}{4} + \frac{x}{2})\sin^{1-\alpha}(\frac{\pi}{4} - \frac{x}{2})$ (see Appendix B). In Appendix B we show that $f(x)$ takes a maximum value when

$$x_* = \arcsin(2\alpha - 1), \tag{59}$$

which leads to Eq. (42) and $\lambda_1 = -\ln f(x_*)$ if x_*/gt is an integer. If x_*/gt is not an integer, we instead have

$$\lambda_1 = -\ln f(gtL), \tag{60}$$

with $L = \mathrm{round}(x_*/gt)$.

Next, since $f(x)$ is a concave function taking the maximum at $x = x_*$ (Appendix B) and S_x takes integer values, we can evaluate λ_2 as

$$\lambda_2 = -\ln f(gtL + gt) \tag{61}$$

or

$$\lambda_2 = -\ln f(gtL - gt). \tag{62}$$

Let us first assume that x_*/gt is an integer, i.e., $gtL = x_*$. Then, assuming $gt \ll 1$, we can evaluate the gap at the leading order of $(gt)^2$ from the form of $f(x)$, finding

$$\lambda_2 - \lambda_1 \simeq \frac{(gt)^2}{4}. \tag{63}$$

This leads to the relaxation timescale

$$m_{\rm relax} \simeq \frac{4}{(gt)^2}. \tag{64}$$

Interestingly, this does not explicitly depend on α.

When x_*/gt is not an integer, the gap becomes smaller than $(gt)^2/4$ but remains the order of $(gt)^2$, unless it accidentally vanishes. Therefore, we conclude that the relaxation time for most measurement outcomes becomes the order of $m_{\rm relax} \sim (gt)^{-2}$.

VI. NUMERICAL SIMULATIONS

In this section we study the case of finite temperature using numerical simulations. The initial state of the spin ensemble is a mixed state, i.e., a thermal equilibrium state subjected to a magnetic field h along the z axis. The quantity that we mainly focus on is

$$C_{\rm cat}(\hat{S}_z, \hat{\rho}_{\rm P}(m)) := \tfrac{1}{2}\|[\hat{S}_z, [\hat{S}_z, \hat{\rho}_{\rm P}(m)]]\|_1. \tag{65}$$

If it is $\Theta(N^q)$ with $q > 1.5$, the state is a SQL-beating catlike state, as discussed in Sec. III. To visualize the emergence of generalized cat states, we numerically compute the value of $C_{\rm cat}(\hat{S}_z, \hat{\rho}_{\rm P}(m))$ for each m up to $m = 1000$. In the following, we take $1/\beta = 0.1$ and $h = 0.5$. The interaction strength between the FQ and the spin ensemble is set to be $gt = 0.222$. This is the case where $gtN > \pi/2$, which we did not analytically discuss above. Remarkably, we can see the emergence of SQL-beating catlike state even in this regime.

A. Trajectories for a fixed N

Let us examine a single trajectory for a fixed N (=15), depicted in Fig. 4. In each trajectory, the measurement outcome at each m is probabilistically determined, and the measurement backaction from each result influences the value of $C_{\rm cat}(\hat{S}_z, \hat{\rho}_{\rm P}(m))$. Due to the stochastic nature of these measurements, a single trajectory exhibits temporal fluctuations, albeit with an overall tendency for $C_{\rm cat}(\hat{S}_z, \hat{\rho}_{\rm P}(m))$ to increase. By averaging over 3000 trajectories, we observe that the value of $C_{\rm cat}(\hat{S}_z, \hat{\rho}_{\rm P}(m))$ undergoes rapid changes initially but becomes almost constant around $m \sim 600$, as shown in the inset of Fig. 4. Note that at $m_{\rm relax} \simeq 4/(gt)^2 \simeq 82$, the value of $C_{\rm cat}(\hat{S}_z, \hat{\rho}_{\rm P}(m))$ is 147, which is nearly half of the stationary value of $C_{\rm cat}(\hat{S}_z, \hat{\rho}_{\rm P}(m))$, even though we consider here the case $gtN > \pi/2$.

B. Scaling behavior of $C_{\rm cat}(\hat{S}_z, \hat{\rho}_{\rm P}(m))$

To determine whether we have successfully created a generalized cat state, it is essential to examine the scaling behavior of the $C_{\rm cat}(\hat{S}_z, \hat{\rho}_{\rm P}(m))$ with respect to N at each m. For $N = 3, 5, 7, 15, 31, 63, 127$, we average 3000 random trajectories and plot the value of $C_{\rm cat}(\hat{S}_z, \hat{\rho}_{\rm P}(m))$ in Fig. 5. A linear fit is performed to determine the slope of the line, corresponding to the index q. As depicted, the slope increases with m, but does not show a significant change after $m \sim 600$.

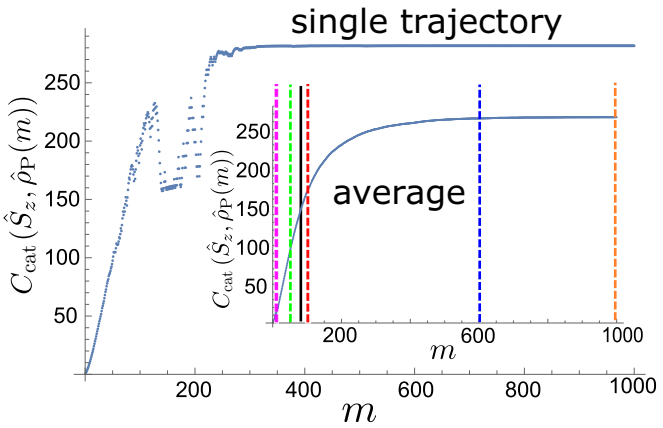

FIG. 4. Visualization of the creation of generalized cat states through repetitive measurements with $N = 15$ qubits. The horizontal axis represents the number of measurements with the FQ, while the vertical axis denotes the value of $C_{\rm cat}(\hat{S}_z, \hat{\rho}_{\rm P}(m))$. Due to the probabilistic nature of each measurement, the values of $C_{\rm cat}(\hat{S}_z, \hat{\rho}_{\rm P}(m))$ exhibit temporal fluctuations within a single trajectory. The inset illustrates the results averaged over 3000 runs. In the inset, the black vertical line shows $m = 82 \simeq m_{\rm relax}$. Purple, green, red, blue, and orange lines in the inset indicate $m = 10, 50, 100, 600, 1000$, respectively. This average reveals a clear, gradual increase in $C_{\rm cat}(\hat{S}_z, \hat{\rho}_{\rm P}(m))$. The initial state is $\exp(-\beta h\hat{S}_z)/{\rm Tr}\exp(-\beta h\hat{S}_z)$, with $1/\beta = 0.1$, $h = 0.5$, and a coupling strength multiplied by the interaction time given by $gt = 0.222$.

With a linear fit using the data for $N = 3, 5, 7, 15, 31, 63, 127$, we obtain up to $q = 1.94$ at $m = 1000$, which is sufficiently close to the generalized cat state with $q = 2$. Since $q > 1.5$ is achieved already for $m = 50$, we can create SQL-beating catlike states by this timescale.

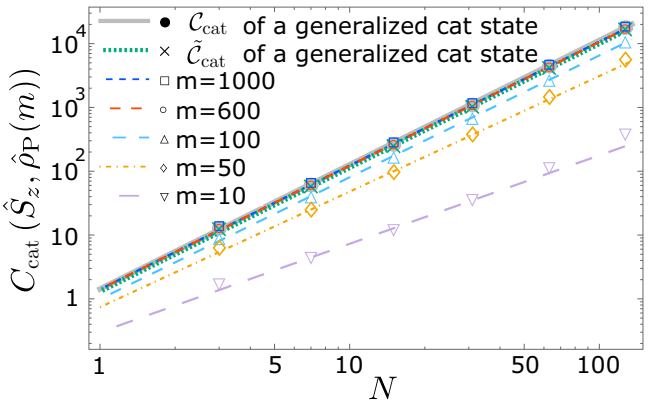

FIG. 5. A log-log plot of the value of $C_{\rm cat}(\hat{S}_z, \hat{\rho}_{\rm P}(m))$ against N for different m values, along with two reference plots. From the bottom to the top, the m values are $m = 10$ (purple), 50 (orange), 100 (cyan), 600 (red), and 1000 (blue). The initial state is given by $\exp(-\beta h\hat{S}_z)/{\rm Tr}\exp(-\beta h\hat{S}_z)$, with $1/\beta = 0.1$, $h = 0.5$, and a coupling strength of $gt = 0.222$. The thick gray line represents the reference obtained from Eq. (66), which is $\mathcal{C}_{\rm cat}$ of a generalized cat state. The green dotted line represents the reference value of $\tilde{\mathcal{C}}_{\rm cat}$ obtained from Eq. (68). Error bars were omitted as they were smaller than the widths of the dots.

Note that, for reference, Fig. 5 also shows two additional curves which concern a generalized cat state $\hat{\rho}_{\rm PM}$ obtained by a single projective measurement $\hat{\mathcal{P}}(M)$ [60] (see Sec. II B), where the initial state is the zero-temperature pure state $\hat{\rho}_{\rm pure} = |{\uparrow}\rangle^{\otimes N}\langle{\uparrow}|^{\otimes N}$. One curve describes $C_{\rm cat}(\hat{S}_z, \hat{\rho}_{\rm PM})$ of the postmeasurement state averaged over outcomes $M = -N, -N+2, \ldots, N$ for the projection measurement,

$$\mathcal{C}_{\rm cat} := \sum_{M=-N,N-2,\ldots,N} \frac{1}{2^N}\binom{N}{\frac{N+M}{2}} \times \frac{\|[\hat{S}_z, [\hat{S}_z, \hat{\mathcal{P}}(M)\hat{\rho}_{\rm pure}\hat{\mathcal{P}}(M)]]\|_1}{2}, \tag{66}$$

where $\binom{N}{(N+M)/2}/2^N$ is the corresponding probability. If the initial state is a mixed state at finite temperature, the average value of $C_{\rm cat}(\hat{S}_z, \hat{\rho}_{\rm PM})$ is smaller than $\mathcal{C}_{\rm cat}$. The second curve is associated with

$$\tilde{\mathcal{C}}_{\rm cat}(\hat{S}_z, \hat{\rho}_{\rm PM}) := {\rm Tr}\{\hat{\mathcal{P}}(M)[\hat{S}_z, [\hat{S}_z, \hat{\rho}_{\rm PM}]]\}, \tag{67}$$

which provides the analytically tractable lower bound of Eq. (65). Motivated by the intuitive measurement protocol explained in Sec. II B, $\tilde{\mathcal{C}}_{\rm cat}$ is defined as the zero-temperature limit ($\beta \to \infty$) of Eq. (5) averaged over all measurement outcomes, i.e.,

$$\begin{aligned}\tilde{\mathcal{C}}_{\rm cat} &:= \sum_{M=-N,N-2,\ldots,N} \frac{1}{2^N}\binom{N}{\frac{N+M}{2}}{\rm Tr}\{\hat{\mathcal{P}}(M)[\hat{S}_z, [\hat{S}_z, \hat{\rho}_{\rm PM}]]\} \\ &= \sum_{M=-N,N-2,\ldots,N} \frac{1}{2^N}\binom{N}{\frac{N+M}{2}}(N^2 - M^2 + 2N).\end{aligned} \tag{68}$$

As can be seen in Fig. 5, the fitted line of the state after 600 measurements is indistinguishable from $\mathcal{C}_{\rm cat}$ and $\tilde{\mathcal{C}}_{\rm cat}$, the plots for the generalized cat state generated via single projective measurement at zero temperature. This implies that the repetitive measurements we consider in this paper can indeed replace the single-projective-measurement scheme in Ref. [60], which required considerably high-resolution measurement. It is also remarkable that our scheme is comparable to the single-projective-measurement scheme under zero temperature, even though we consider nonzero temperature.

Finally, we note that within this numerical simulation, we cannot achieve $\Theta(N^2)$ scaling of $C_{\rm cat}(\hat{S}_z, \hat{\rho}_{\rm P}(m))$ from the fitting. The possible reasons for this are as follows. First, we considered the region $gtN > \pi/2$ in the numerical simulation, while we proved (57) assuming $gtN < \pi/2$. Second, unless N is infinitely large, there will be a finite contribution from both $\Theta(N^2)$ and $\Theta(N)$ terms even when the generalized cat states are considered, as can be seen in Eq. (5). When we substitute $N = 3, 5, 7, 15, 31, 63, 127$ in Eqs. (66) and (68) and perform the linear fitting in the same manner, we obtain $q = 1.95$, which is less than 2, even when accounting for fitting error [91]. Consequently, it is challenging to obtain $C_{\rm cat}(\hat{S}_z, \hat{\rho}_{\rm P}(m))$ with the scaling $\Theta(N^2)$ from numerical simulations up to $N = 127$. Nonetheless, our results are still significant as they demonstrate the potential of utilizing this highly entangled state with $q > 1.5$ for quantum sensing, as we discussed above.

TABLE I. Comparison of sensitivity of states with various q. The uncertainty $\delta\omega$ for states with $q = 1, 1.81, 1.91, 1.94, 2$ is calculated. We can see a clear advantage of $q > 1.5$.

m	q	$\delta\omega$
	1 (separable state)	$4.4 \times 10^{-2}/\sqrt{Tt_{\rm int}}$
50	1.81	$\leqslant 2.4 \times 10^{-2}/\sqrt{Tt_{\rm int}}$
100	1.91	$\leqslant 1.2 \times 10^{-2}/\sqrt{Tt_{\rm int}}$
600	1.94	$\leqslant 7.4 \times 10^{-3}/\sqrt{Tt_{\rm int}}$
	2 (generalized cat state)	$\leqslant 7.0 \times 10^{-3}/\sqrt{Tt_{\rm int}}$

C. Sensitivity of the generated states

Let us calculate the sensitivity of the states with $q > 1.5$ that are generated through the repetitive measurements. We consider the case where $N = 127$. Substituting the value of $C_{\rm cat}(\hat{S}_z, \hat{\rho}_{\rm P}(m))$ for Eq. (20), we show $\delta\omega$ of the following states in Table I: the state at $m = 50$ with $q = 1.81$, the state at $m = 100$ with $q = 1.91$, the state at $m = 600$ with $q = 1.94$, and the generalized cat state with $q = 2$ obtained by a single projective measurement. We also calculate the sensitivity of a separable state using a known formula $\delta\omega = \frac{1}{2\sqrt{N}\sqrt{Tt_{\rm int}}}$.

From this table it is clear that states with $q > 1.5$, produced via a moderate number of measurements, are indeed more advantageous in quantum sensing than a separable state.

VII. CONCLUSION AND OUTLOOK

We studied the relation between $\delta\omega$ and q and derived an inequality $\delta\omega \leqslant O(N^{1-q})$. Any state with $q > 1.5$ is advantageous in quantum metrology, hence we call states with $q > 1.5$ SQL-beating catlike states. We proposed a method to create SQL-beating catlike states through repetitive measurements. A thermal equilibrium state of the spin ensemble was coupled with an ancillary qubit, and we repeatedly measured the ancillary qubits. This sequential measurement of the ancillary qubit provides information about the total magnetization of the spins, leading the spin ensemble to gradually approach the SQL-beating catlike states. Notably, no dynamical control over the spin ensembles is required during the creation of these states. Analytically, we demonstrated that the final state is likely to become a SQL-beating catlike state when the initial state is pure, i.e., at zero temperature. For a mixed state at finite temperature as the initial state, we numerically showed that SQL-beating catlike states can be created via repetitive measurements. We discussed the feasibility of our proposal concerning a hybrid system of an electron spin ensemble and superconducting flux qubit, strengthening the connection between quantum metrology and quantum computing. These results pave the way for the realization of entanglement-enhanced metrology.

In the future work, it would be interesting to speed up the generation of SQL-beating catlike states, since cat states are fragile in general. Recently, utilization of shortcuts to adiabaticity (STA) has been studied for quick generation of metrologically useful states, i.e., NOON states and spin squeezed states [92–94]. Since our scheme includes measurements, it is nontrivial how we can speed up the generation. Still, since the STA formalism is widely studied and it is even extended to open quantum systems [95], it would be interesting to pursue the application of this formalism to our scheme.

ACKNOWLEDGMENTS

M.T. was supported by the Japan Society for the Promotion of Science through a JSPS fellowship (JSPS KAKENHI Grant No. 22KJ3175). This work was supported by JST Moonshot (Grant No. JPMJMS226C). Y.M. was supported by JSPS KAKENHI (Grant No. 23H04390). This work was supported by CREST (Grants No. JPMJCR23I5 and No. 20H05661), JST. This work was supported by JST Moonshot (Grant No. JPMJMS226C) and Presto JST (Grant No. JPMJPR245B). R.H. was supported by JST ERATO Grant No. JPMJER2302, Japan, and JSPS KAKENHI Grant No. JP24K16982. A.S. was supported by Japan Society for the Promotion of Science KAKENHI Grant No. 23K22413 and by the RIKEN TRIP initiative.

DATA AVAILABILITY

The data that support the findings of this article are openly available in Ref. [96].

APPENDIX A: DERIVATION OF THE STATE AFTER THE $(m+1)$th MEASUREMENT

Let us investigate $\hat{\rho}_{\rm P}(m+1)$, the state after the $(m+1)$th measurement, from $\hat{\rho}_{\rm P}(m)$. The measurement protocol is as follows. First, we initialize the FQ so that the initial state is $\hat{\rho}_{\rm P}(m) \otimes |+\rangle\langle+|$. Then we let the total state evolve with the Hamiltonian $\hat{H}_{\rm R} = \frac{g}{2}\hat{S}_x \otimes \hat{\Sigma}_3$. Finally, we read out the FQ on the $\hat{\Sigma}_2$ basis ($\hat{\Sigma}_2|\pm_y\rangle = |\pm_y\rangle$). If we obtain $+1$ as an outcome of the measurement, then $\hat{\rho}_{\rm P}(m+1) = \hat{\rho}_{\rm P}(m+1)_+$, which is written as

$$\hat{\rho}_{\rm P}(m+1)_+ = \frac{\langle+_y|e^{-i(g/2)\hat{S}_x\otimes\hat{\Sigma}_3 t}\hat{\rho}_{\rm P}(m)\otimes|+\rangle\langle+|e^{i(g/2)\hat{S}_x\otimes\hat{\Sigma}_3 t}|+_y\rangle}{\mathrm{Prob}(\Sigma_2=+1)} \tag{A1}$$

$$= \frac{\hat{W}_+\hat{\rho}_{\rm P}(m)\hat{W}_+^\dagger}{\mathrm{Prob}(\Sigma_2=+1)}, \tag{A2}$$

where

$$\hat{W}_+ = \langle+_y|e^{-i(g/2)\hat{S}_x\otimes\hat{\Sigma}_3 t}|+\rangle \tag{A3}$$

$$= \frac{e^{-i(g/2)t\hat{S}_x} - ie^{i(g/2)t\hat{S}_x}}{2} \tag{A4}$$

$$= \frac{1-i}{\sqrt{2}}\sin\left(\frac{\pi}{4}+\frac{gt}{2}\hat{S}_x\right) \tag{A5}$$

and

$$\mathrm{Prob}(\Sigma_2=+1) = \mathrm{Tr}[\langle+_y|e^{-i(g/2)\hat{S}_x\otimes\hat{\Sigma}_3 t}\hat{\rho}_{\rm P}(m)\otimes|+\rangle\langle+|e^{i(g/2)\hat{S}_x\otimes\hat{\Sigma}_3 t}|+_y\rangle]. \tag{A6}$$

Similarly, if we obtain -1 as an outcome of the measurement, then $\hat{\rho}_{\rm P}(m+1) = \hat{\rho}_{\rm P}(m+1)_-$, which is written as

$$\hat{\rho}_{\rm P}(m+1)_- = \frac{\langle -_y|e^{-i(g/2)\hat{S}_x\otimes\hat{\Sigma}_3 t}\hat{\rho}_{\rm P}(m)\otimes|+\rangle\langle+|e^{i(g/2)\hat{S}_x\otimes\hat{\Sigma}_3 t}|-_y\rangle}{\mathrm{Prob}(\Sigma_2=-1)} \tag{A7}$$

$$= \frac{\hat{W}_-\hat{\rho}_{\rm P}(m)\hat{W}_-^\dagger}{\mathrm{Prob}(\Sigma_2=-1)}, \tag{A8}$$

where

$$\hat{W}_- = \langle -_y|e^{-i(g/2)\hat{S}_x\otimes\hat{\Sigma}_3 t}|+\rangle \tag{A9}$$

$$= \frac{e^{-i(g/2)t\hat{S}_x} + ie^{i(g/2)t\hat{S}_x}}{2} \tag{A10}$$

$$= \frac{1+i}{\sqrt{2}}\sin\left(\frac{\pi}{4} - \frac{gt}{2}\hat{S}_x\right) \tag{A11}$$

and

$$\mathrm{Prob}(\Sigma_2=-1) = \mathrm{Tr}[\langle -_y|e^{-i(g/2)\hat{S}_x\otimes\hat{\Sigma}_3 t}\hat{\rho}_{\rm P}(m)\otimes|+\rangle\langle+|e^{i(g/2)\hat{S}_x\otimes\hat{\Sigma}_3 t}|-_y\rangle]. \tag{A12}$$

APPENDIX B: DERIVATION OF $|\phi_m\rangle$

Here let us discuss the state we get after applying $\hat{W}_+^k\hat{W}_-^{m-k}$, where $0 \leqslant k \leqslant m$ is the number of $\hat{W}_+$ applied in m measurements. There is a theorem that when an operator $\hat{K}$ is applied infinite times, the state converges to the eigenstate of $\hat{K}$ with the eigenvalue whose modulus is the largest, provided it is nondegenerate. Furthermore, in our case, for $k = \alpha m$ where $0 < \alpha < 1$, we obtain $(\hat{W}_+)^k(\hat{W}_-)^{m-k} = [(\hat{W}_+)^\alpha(\hat{W}_-)^{(1-\alpha)}]^m$. By taking $\hat{K} := (\hat{W}_+)^\alpha(\hat{W}_-)^{(1-\alpha)}$, we can adopt this theorem.

We want to find the largest (in magnitude) eigenvalue of

$$\hat{K} = \left[\frac{1-i}{\sqrt{2}}\sin\left(\frac{\pi}{4}+\frac{gt}{2}\hat{S}_x\right)\right]^\alpha\left[\frac{1+i}{\sqrt{2}}\sin\left(\frac{\pi}{4}-\frac{gt}{2}\hat{S}_x\right)\right]^{1-\alpha} \tag{B1}$$

for each α. When $\hat{K}$ is applied to some initial state $|\psi_0\rangle = \sum_l c_l|S_x = l\rangle$, then

$$\hat{K}|\psi_0\rangle = \left(\frac{1-i}{\sqrt{2}}\right)^\alpha\left(\frac{1+i}{\sqrt{2}}\right)^{1-\alpha}\sin^\alpha\left(\frac{\pi}{4}+\frac{gt}{2}\hat{S}_x\right) \times \sin^{1-\alpha}\left(\frac{\pi}{4}-\frac{gt}{2}\hat{S}_x\right)\sum_l c_l|S_x=l\rangle \tag{B2}$$

$$= \left(\frac{1-i}{\sqrt{2}}\right)^\alpha\left(\frac{1+i}{\sqrt{2}}\right)^{1-\alpha}\sum_l c_l\sin^\alpha\left(\frac{\pi}{4}+\frac{gt}{2}l\right) \times \sin^{1-\alpha}\left(\frac{\pi}{4}-\frac{gt}{2}l\right)|S_x=l\rangle. \tag{B3}$$

Let us define $f(x)$ as

$$f(x) := \sin^\alpha\left(\frac{\pi}{4}+\frac{x}{2}\right)\sin^{1-\alpha}\left(\frac{\pi}{4}-\frac{x}{2}\right). \tag{B4}$$

TABLE II. Derivative test chart of $f(x)$, which increases (+) until $x = \arcsin(2\alpha-1)$ and then decreases (−).

x	$-\pi/2$	$\arcsin(2\alpha-1)$	$\pi/2$
$f'(x)$	+	0	−
$f(x)$	↗		↘

Finding the extremum of $f(x)$ corresponds to finding the largest eigenvalue of $\hat{K}$ because $\hat{W}_\pm$ are diagonal in the $\hat{S}_x$ basis.

To find the extremum, we take the derivative

$$f'(x) = \frac{2\alpha - 1 - \sin x}{4\sin^{1-\alpha}\left(\frac{\pi}{4}+\frac{x}{2}\right)\sin^\alpha\left(\frac{\pi}{4}-\frac{x}{2}\right)}. \tag{B5}$$

We can see that $f(x)$ takes the extremum at x that satisfies $g(x) = 0$, where

$$g(x) := 2\alpha - 1 - \sin x. \tag{B6}$$

It is obvious that $g(x)$ takes zero at

$$\sin x = 2\alpha - 1. \tag{B7}$$

For simplicity, let us first consider the region

$$-\frac{\pi}{2} < x < \frac{\pi}{2}. \tag{B8}$$

Since $0 < \alpha < 1$, $f(x)$ takes the maximum at $x = \arcsin(2\alpha-1)$, which is greater than zero and smaller than $\pi/2$. When $\alpha = 1$ (-1), $f(x)$ takes the maximum (minimum) 1 (-1) at $x = \pi/2$ $(-\pi/2)$. These are illustrated as in Table II.

Therefore, under the assumption $-\pi/2 < x < \pi/2$, the function $f(x)$ takes the maximum at $x = \arcsin(2\alpha-1)$, leading to the conclusion that after applying $\hat{K}$ for $m \gg 1$ times, the final state $|\phi_m\rangle$ approaches (42).

Let us also consider the case of $x \geqslant \pi/2$ or $x \leqslant -\pi/2$. In general, $g(x)$ takes zero at

$$x = \arcsin(2\alpha-1) + 2n\pi, \tag{B9}$$

$$x = \pi - \arcsin(2\alpha-1) + 2n\pi, \tag{B10}$$

where $n \in \mathbb{Z}$. Actually, we can prove that

$$|f(x)| = (1-\alpha)^{(1-\alpha)/2}(\alpha)^{\alpha/2} \tag{B11}$$

$$= \sqrt{(1-\alpha)^{1-\alpha}\alpha^\alpha} \tag{B12}$$

for any x that satisfies $g(x) = 0$, i.e., $\sin x = 2k/m - 1$. With the extrema with the equal value of $|f(x)|$, this implies that there are multiple candidates for the final state. In such a case, we should consider the weight of the eigenstates that are candidates for the final state, in the initial state. In other words, the final state should be the superposition of the candidates whose weight is determined by the initial state.

APPENDIX C: DERIVATION OF $p(k)$

Here we explain the derivation of $p(k)$, the probability of obtaining the trajectory with $\hat{W}_+$ applied k times:

$$(\hat{W}_+^\dagger \hat{W}_+)^k (\hat{W}_-^\dagger \hat{W}_-)^{m-k} = \left[\sin^2\left(\frac{\pi}{4}+\frac{gt}{2}\hat{S}_x\right)\right]^k \left[\sin^2\left(\frac{\pi}{4}-\frac{gt}{2}\hat{S}_x\right)\right]^{m-k} \quad \text{(C1)}$$

$$= \left(\frac{1+\sin(gt\hat{S}_x)}{2}\right)^k \left(\frac{1-\sin(gt\hat{S}_x)}{2}\right)^{m-k}. \quad \text{(C2)}$$

We use $|S_x = 2r - N\rangle$ (where $r = 0, 1, \ldots, N$ is the number of up spins) in (44) as

$$|S_x = 2r - N\rangle = \left|D_N^{(\theta)}\right\rangle = \sqrt{\binom{N}{\frac{N+\theta}{2}}^{-1}} \sum_{\sigma\in\mathcal{S}_N} \mathcal{P}_\sigma(|+\rangle^{\otimes(N+\theta)/2}|-\rangle^{\otimes(N-\theta)/2}), \quad \text{(C3)}$$

with $\theta = 2r - N$. Importantly,

$$|\uparrow\rangle^{\otimes N} = \left(\frac{|+\rangle+|-\rangle}{\sqrt{2}}\right)^{\otimes N} = \frac{1}{\sqrt{2^N}} \sum_{r=0}^{N} |S_x = 2r-N\rangle \sqrt{\binom{N}{r}}. \quad \text{(C4)}$$

Hence we obtain

$$p(k) = \binom{m}{k} \langle\uparrow|^{\otimes N} (\hat{W}_+^\dagger \hat{W}_+)^k (\hat{W}_-^\dagger \hat{W}_-)^{m-k} |\uparrow\rangle^{\otimes N} \quad \text{(C5)}$$

$$= \binom{m}{k} \frac{1}{2^N} \sum_{r=0}^{N} \langle S_x = 2r-N| \sqrt{\binom{N}{r}} \times \left(\frac{1+\sin(gt\hat{S}_x)}{2}\right)^k \left(\frac{1-\sin(gt\hat{S}_x)}{2}\right)^{m-k} \times \sum_{r'=0}^{N} |S_x = 2r'-N\rangle \sqrt{\binom{N}{r'}} \quad \text{(C6)}$$

$$= \binom{m}{k} \frac{1}{2^N} \sum_{r=0}^{N} \binom{N}{r} \times \left(\frac{1+\sin[gt(2r-N)]}{2}\right)^k \times \left(\frac{1-\sin[gt(2r-N)]}{2}\right)^{m-k}. \quad \text{(C7)}$$

APPENDIX D: PROBABILITY OF OBTAINING A GENERALIZED CAT STATE

We consider the case where m is even. Here we discuss the probablity of obtaining a generalized cat state after m measurements with $|\uparrow\rangle^{\otimes N}$ as an initial state. We take the sum of $p(k)$ over k, which allows the emergence of generalized cat states, and prove that it converges to 1 in the limit $N \to \infty$ (note that we take $N \to \infty$ after $m \to \infty$). The probability $p(k)$ can be regarded as a sum of binomial distributions with weight $\binom{N}{r}/2^N$,

$$p(k) = \frac{1}{2^N} \sum_{r=0}^{N} \binom{N}{r} B(gt, r, k), \quad \text{(D1)}$$

$$B(gt, r) := \binom{m}{k} s(gt, r)^k [1 - s(gt, r)]^{m-k}, \quad \text{(D2)}$$

$$s(gt, r) := \frac{1+\sin[gt(2r-N)]}{2}. \quad \text{(D3)}$$

If we assume $gtN < \pi/2$, we find $s(gt, r) > 0$ and $1 - s(gt, r) > 0$. Since we are considering large m, the binomial distribution $B(gt, r)$ can be approximated as the normal distribution, i.e.,

$$B(gt, r, k) \simeq \frac{1}{\sqrt{2\pi m s(gt, r)[1 - s(gt, r)]}} \times \exp\left(-\frac{[k - ms(gt, r)]^2}{2ms(gt, r)[1 - s(gt, r)]}\right); \quad \text{(D4)}$$

$$\therefore p(k) \simeq \frac{1}{2^N} \sum_{r=0}^{N} \binom{N}{r} \frac{1}{\sqrt{2\pi m s(gt, r)[1 - s(gt, r)]}} \times \exp\left(-\frac{[k - ms(gt, r)]^2}{2ms(gt, r)[1 - s(gt, r)]}\right). \quad \text{(D5)}$$

Note that $s(gt, r)$ is a monotonically increasing function of r.

Consider the sum of $p(k)$ from $k = m\alpha_1$ to $k = m\alpha_2$. When $m \gg 1$, we can replace the sum with integral, i.e.,

$$\sum_{k=m\alpha_1}^{m\alpha_2} p(k) = \sum_{k=m\alpha_1}^{m\alpha_2} \frac{1}{2^N} \sum_{r=0}^{N} \binom{N}{r} B(gt, r, k) \quad \text{(D6)}$$

$$\simeq \frac{1}{2^N} \sum_{r=0}^{N} \binom{N}{r} \sqrt{\frac{m}{2\pi s(gt, r)[1 - s(gt, r)]}} \times \int_{\alpha_1}^{\alpha_2} d\alpha \exp\left(-\frac{[\alpha - s(gt, r)]^2}{2s(gt, r)[1 - s(gt, r)]} m\right) \quad \text{(D7)}$$

$$\to \frac{1}{2^N} \sum_{r=0}^{N} \binom{N}{r} \int_{\alpha_1}^{\alpha_2} d\alpha\, \delta(\alpha - s(gt, r)), \quad \text{(D8)}$$

where the limit in the last line is for $m \to \infty$. Here we substitute $\gamma = \sqrt{\frac{s(gt,r)[1-s(gt,r)]}{m}}$ into the following known formula:

$$\lim_{\gamma\to 0} \frac{\exp\left(-\frac{x^2}{2\gamma^2}\right)}{\sqrt{2\pi}\gamma} = \delta(x). \quad \text{(D9)}$$

Let us take $\alpha_1 = s(gt, r_1)$ and $\alpha_2 = s(gt, r_2)$. Then the integral is further simplified as follows:

$$\sum_{k=ms(gt,r_1)}^{ms(gt,r_2)} p(k) \simeq \frac{1}{2^N} \sum_{r=r_1}^{r_2} \binom{N}{r}. \quad \text{(D10)}$$

Now, to evaluate the lower bound of the probability of the emergence of the generalized cat states, we can take $r_1 = Nx_1$ and $r_2 = Nx_2$ with $0 < x_1 < 1/2 < x_2 < 1$ in the above equation. To see that this choice is appropriate, we substitute $k = ms(gt, \tilde{r})$ into Eq. (42), finding

$$|\phi_m\rangle = |S_x = 2\tilde{r} - N\rangle. \quad \text{(D11)}$$

According to Eq. (54), this means that the final state $|\phi_m\rangle$ is indeed a generalized cat state for any $\tilde{r} = Nx$ with $0 < x < 1$.

Then we finally have

$$\sum_{k=ms(gt,r_1)}^{ms(gt,r_2)} p(k) = \frac{1}{2^N} \sum_{r=Nx_1}^{Nx_2} \binom{N}{r} \tag{D12}$$

$$\simeq \sum_{r=Nx_1}^{Nx_2} \sqrt{\frac{2}{\pi N}} \exp\left(-\frac{2(r-N/2)^2}{N}\right) \tag{D13}$$

$$\to \int_{x_1}^{x_2} dx\, \delta(x-1/2) \quad (N \to \infty). \tag{D14}$$

Here we approximated the binomial distribution in the same manner as we did with $B(gt, r, k)$, assuming $N \gg 1$. We can immediately see that this approaches 1 in the limit $N \to \infty$. Therefore, the probability of obtaining a generalized cat state after infinitely many measurements is 1 with $N \to \infty$.

[1] V. Giovannetti, S. Lloyd, and L. Maccone, Quantum-enhanced measurements: Beating the standard quantum limit, Science **306**, 1330 (2004).

[2] V. Giovannetti, S. Lloyd, and L. Maccone, Advances in quantum metrology, Nat. Photon. **5**, 222 (2011).

[3] M. A. Taylor and W. P. Bowen, Quantum metrology and its application in biology, Phys. Rep. **615**, 1 (2016).

[4] C. L. Degen, F. Reinhard, and P. Cappellaro, Quantum sensing, Rev. Mod. Phys. **89**, 035002 (2017).

[5] D. J. Wineland, J. J. Bollinger, W. M. Itano, F. L. Moore, and D. J. Heinzen, Spin squeezing and reduced quantum noise in spectroscopy, Phys. Rev. A **46**, R6797 (1992).

[6] D. J. Wineland, J. J. Bollinger, W. M. Itano, and D. J. Heinzen, Squeezed atomic states and projection noise in spectroscopy, Phys. Rev. A **50**, 67 (1994).

[7] G. Tóth and I. Apellaniz, Quantum metrology from a quantum information science perspective, J. Phys. A: Math. Theor. **47**, 424006 (2014).

[8] M. G. Paris, Quantum estimation for quantum technology, Int. J. Quantum Inf. **07**, 125 (2009).

[9] A. W. Chin, S. F. Huelga, and M. B. Plenio, Quantum metrology in non-Markovian environments, Phys. Rev. Lett. **109**, 233601 (2012).

[10] R. Chaves, J. B. Brask, M. Markiewicz, J. Kołodyński, and A. Acín, Noisy metrology beyond the standard quantum limit, Phys. Rev. Lett. **111**, 120401 (2013).

[11] J. A. Jones, S. D. Karlen, J. Fitzsimons, A. Ardavan, S. C. Benjamin, G. A. D. Briggs, and J. J. Morton, Magnetic field sensing beyond the standard quantum limit using 10-spin NOON states, Science **324**, 1166 (2009).

[12] S. F. Huelga, C. Macchiavello, T. Pellizzari, A. K. Ekert, M. B. Plenio, and J. I. Cirac, Improvement of frequency standards with quantum entanglement, Phys. Rev. Lett. **79**, 3865 (1997).

[13] A. Kuzmich, N. Bigelow, and L. Mandel, Atomic quantum nondemolition measurements and squeezing, Europhys. Lett. **42**, 481 (1998).

[14] M. Fleischhauer, A. Matsko, and M. O. Scully, Quantum limit of optical magnetometry in the presence of ac Stark shifts, Phys. Rev. A **62**, 013808 (2000).

[15] J. M. Geremia, J. K. Stockton, A. C. Doherty, and H. Mabuchi, Quantum Kalman filtering and the Heisenberg limit in atomic magnetometry, Phys. Rev. Lett. **91**, 250801 (2003).

[16] D. Leibfried, M. D. Barrett, T. Schaetz, J. Britton, J. Chiaverini, W. M. Itano, J. D. Jost, C. Langer, and D. J. Wineland, Toward Heisenberg-limited spectroscopy with multiparticle entangled states, Science **304**, 1476 (2004).

[17] M. Auzinsh, D. Budker, D. F. Kimball, S. M. Rochester, J. E. Stalnaker, A. O. Sushkov, and V. V. Yashchuk, Can a quantum nondemolition measurement improve the sensitivity of an atomic magnetometer? Phys. Rev. Lett. **93**, 173002 (2004).

[18] J. A. Dunningham, Using quantum theory to improve measurement precision, Contemp. Phys. **47**, 257 (2006).

[19] Y. Matsuzaki, S. C. Benjamin, and J. Fitzsimons, Magnetic field sensing beyond the standard quantum limit under the effect of decoherence, Phys. Rev. A **84**, 012103 (2011).

[20] R. Demkowicz-Dobrzański, J. Kołodyński, and M. Guţă, The elusive Heisenberg limit in quantum-enhanced metrology, Nat. Commun. **3**, 1063 (2012).

[21] J. G. Bohnet, K. C. Cox, M. A. Norcia, J. M. Weiner, Z. Chen, and J. K. Thompson, Reduced spin measurement back-action for a phase sensitivity ten times beyond the standard quantum limit, Nat. Photon. **8**, 731 (2014).

[22] T. Tanaka, P. Knott, Y. Matsuzaki, S. Dooley, H. Yamaguchi, W. J. Munro, and S. Saito, Proposed robust entanglement-based magnetic field sensor beyond the standard quantum limit, Phys. Rev. Lett. **115**, 170801 (2015).

[23] S. Dooley, E. Yukawa, Y. Matsuzaki, G. C. Knee, W. J. Munro, and K. Nemoto, A hybrid-systems approach to spin squeezing using a highly dissipative ancillary system, New J. Phys. **18**, 053011 (2016).

[24] E. Davis, G. Bentsen, and M. Schleier-Smith, Approaching the Heisenberg limit without single-particle detection, Phys. Rev. Lett. **116**, 053601 (2016).

[25] Y. Matsuzaki, S. Benjamin, S. Nakayama, S. Saito, and W. J. Munro, Quantum metrology beyond the classical limit under the effect of dephasing, Phys. Rev. Lett. **120**, 140501 (2018).

[26] W. Happer and H. Tang, Spin-exchange shift and narrowing of magnetic resonance lines in optically pumped alkali vapors, Phys. Rev. Lett. **31**, 273 (1973).

[27] J. C. Allred, R. N. Lyman, T. W. Kornack, and M. V. Romalis, High-sensitivity atomic magnetometer unaffected by spin-exchange relaxation, Phys. Rev. Lett. **89**, 130801 (2002).

[28] H. Dang, A. C. Maloof, and M. V. Romalis, Ultrahigh sensitivity magnetic field and magnetization measurements with an atomic magnetometer, Appl. Phys. Lett. **97**, 151110 (2010).

[29] M. Bal, C. Deng, J.-L. Orgiazzi, F. Ong, and A. Lupascu, Ultrasensitive magnetic field detection using a single artificial atom, Nat. Commun. **3**, 1324 (2012).

[30] H. Toida, Y. Matsuzaki, K. Kakuyanagi, X. Zhu, W. J. Munro, H. Yamaguchi, and S. Saito, Electron paramagnetic resonance spectroscopy using a single artificial atom, Commun. Phys. **2**, 33 (2019).

[31] V. M. Acosta, E. Bauch, M. P. Ledbetter, C. Santori, K.-M. C. Fu, P. E. Barclay, R. G. Beausoleil, H. Linget, J. F. Roch, F. Treussart, S. Chemerisov, W. Gawlik, and D. Budker, Diamonds with a high density of nitrogen-vacancy centers for magnetometry applications, Phys. Rev. B **80**, 115202 (2009).

[32] G. Balasubramanian, P. Neumann, D. Twitchen, M. Markham, R. Kolesov, N. Mizuochi, J. Isoya, J. Achard, J. Beck, J. Tissler, *et al.*, Ultralong spin coherence time in isotopically engineered diamond, Nat. Mater. **8**, 383 (2009).

[33] F. Dolde, H. Fedder, M. W. Doherty, T. Nöbauer, F. Rempp, G. Balasubramanian, T. Wolf, F. Reinhard, L. C. Hollenberg, F. Jelezko, *et al.*, Electric-field sensing using single diamond spins, Nat. Phys. **7**, 459 (2011).

[34] T. Ishikawa, K.-M. C. Fu, C. Santori, V. M. Acosta, R. G. Beausoleil, H. Watanabe, S. Shikata, and K. M. Itoh, Optical and spin coherence properties of nitrogen-vacancy centers placed in a 100 nm thick isotopically purified diamond layer, Nano Lett. **12**, 2083 (2012).

[35] G. M. Palma, K.-A. Suominen, and A. Ekert, Quantum computers and dissipation, Proc. R. Soc. London A **452**, 567 (1996).

[36] A. Smirne, J. Kołodyński, S. F. Huelga, and R. Demkowicz-Dobrzański, Ultimate precision limits for noisy frequency estimation, Phys. Rev. Lett. **116**, 120801 (2016).

[37] K. Macieszczak, Zeno limit in frequency estimation with non-Markovian environments, Phys. Rev. A **92**, 010102(R) (2015).

[38] W. H. Zurek, Decoherence and the transition from quantum to classical, Phys. Today **44**(10), 36 (1991).

[39] H.-P. Breuer and F. Petruccione, *The Theory of Open Quantum Systems* (Oxford University Press, New York, 2002).

[40] B. Tratzmiller, Q. Chen, I. Schwartz, S. F. Huelga, and M. B. Plenio, Limited-control metrology approaching the Heisenberg limit without entanglement preparation, Phys. Rev. A **101**, 032347 (2020).

[41] E. Schrödinger, Die gegenwärtige situation in der quantenmechanik, Naturwissenschaften **23**, 823 (1935).

[42] D. M. Greenberger, M. A. Horne, A. Shimony, and A. Zeilinger, Bell's theorem without inequalities, Am. J. Phys. **58**, 1131 (1990).

[43] T. Monz, P. Schindler, J. T. Barreiro, M. Chwalla, D. Nigg, W. A. Coish, M. Harlander, W. Hänsel, M. Hennrich, and R. Blatt, 14-qubit entanglement: Creation and coherence, Phys. Rev. Lett. **106**, 130506 (2011).

[44] L. DiCarlo, M. D. Reed, L. Sun, B. R. Johnson, J. M. Chow, J. M. Gambetta, L. Frunzio, S. M. Girvin, M. H. Devoret, and R. J. Schoelkopf, Preparation and measurement of three-qubit entanglement in a superconducting circuit, Nature (London) **467**, 574 (2010).

[45] C. Monroe, D. M. Meekhof, B. E. King, and D. J. Wineland, A "Schrödinger cat" superposition state of an atom, Science **272**, 1131 (1996).

[46] M. Brune, E. Hagley, J. Dreyer, X. Maitre, A. Maali, C. Wunderlich, J.-M. Raimond, and S. Haroche, Observing the progressive decoherence of the "meter" in a quantum measurement, Phys. Rev. Lett. **77**, 4887 (1996).

[47] J. R. Friedman, V. Patel, W. Chen, S. Tolpygo, and J. E. Lukens, Quantum superposition of distinct macroscopic states, Nature (London) **406**, 43 (2000).

[48] D. Leibfried, E. Knill, S. Seidelin, J. Britton, R. B. Blakestad, J. Chiaverini, D. B. Hume, W. M. Itano, J. D. Jost, C. Langer, *et al.*, Creation of a six-atom 'Schrödinger cat' state, Nature (London) **438**, 639 (2005).

[49] A. Ourjoumtsev, H. Jeong, R. Tualle-Brouri, and P. Grangier, Generation of optical 'Schrödinger cats' from photon number states, Nature (London) **448**, 784 (2007).

[50] S. Deleglise, I. Dotsenko, C. Sayrin, J. Bernu, M. Brune, J.-M. Raimond, and S. Haroche, Reconstruction of non-classical cavity field states with snapshots of their decoherence, Nature (London) **455**, 510 (2008).

[51] W.-B. Gao, C.-Y. Lu, X.-C. Yao, P. Xu, O. Gühne, A. Goebel, Y.-A. Chen, C.-Z. Peng, Z.-B. Chen, and J.-W. Pan, Experimental demonstration of a hyper-entangled ten-qubit Schrödinger cat state, Nat. Phys. **6**, 331 (2010).

[52] B. Vlastakis, G. Kirchmair, Z. Leghtas, S. E. Nigg, L. Frunzio, S. M. Girvin, M. Mirrahimi, M. H. Devoret, and R. J. Schoelkopf, Deterministically encoding quantum information using 100-photon Schrödinger cat states, Science **342**, 607 (2013).

[53] G. Kirchmair, B. Vlastakis, Z. Leghtas, S. E. Nigg, H. Paik, E. Ginossar, M. Mirrahimi, L. Frunzio, S. M. Girvin, and R. J. Schoelkopf, Observation of quantum state collapse and revival due to the single-photon Kerr effect, Nature (London) **495**, 205 (2013).

[54] C. Wang, Y. Y. Gao, P. Reinhold, R. W. Heeres, N. Ofek, K. Chou, C. Axline, M. Reagor, J. Blumoff, K. Sliwa, *et al.*, A Schrödinger cat living in two boxes, Science **352**, 1087 (2016).

[55] V. M. Stojanović and J. K. Nauth, Interconversion of W and Greenberger-Horne-Zeilinger states for Ising-coupled qubits with transverse global control, Phys. Rev. A **106**, 052613 (2022).

[56] V. M. Stojanović and J. K. Nauth, Dicke-state preparation through global transverse control of Ising-coupled qubits, Phys. Rev. A **108**, 012608 (2023).

[57] F. Fröwis, P. Sekatski, W. Dür, N. Gisin, and N. Sangouard, Macroscopic quantum states: Measures, fragility, and implementations, Rev. Mod. Phys. **90**, 025004 (2018).

[58] A. Shimizu and T. Morimae, Detection of macroscopic entanglement by correlation of local observables, Phys. Rev. Lett. **95**, 090401 (2005).

[59] We use the notation $\Theta(N^k)$ in addition to the standard notation $O(N^k)$, i.e., $O(N^k)/N^k \to$ const ($\neq 0$) in the limit $N \to \infty$, with the following meaning: For a function g of N, we say $g = \Theta(N^k)$ if g/N^k approaches a positive constant as $N \to \infty$. If $g = \Theta(N^k)$ then $g = O(N^k)$, but the inverse is not necessarily true.

[60] M. Tatsuta and A. Shimizu, Conversion of thermal equilibrium states into superpositions of macroscopically distinct states, Phys. Rev. A **97**, 012124 (2018).

[61] M. Tatsuta, Y. Matsuzaki, and A. Shimizu, Quantum metrology with generalized cat states, Phys. Rev. A **100**, 032318 (2019).

[62] Note that $\hat{a}(l)$ is allowed to be different from the spatial translation of $\hat{a}(l')$ ($l' \neq l$), i.e., $\hat{A}$ may not be translationally invariant.

[63] J. Liu, H. Yuan, X.-M. Lu, and X. Wang, Quantum Fisher information matrix and multiparameter estimation, J. Phys. A: Math. Theor. **53**, 023001 (2020).

[64] A. M. Tyryshkin, S. Tojo, J. J. Morton, H. Riemann, N. V. Abrosimov, P. Becker, H.-J. Pohl, T. Schenkel, M. L. Thewalt, K. M. Itoh, *et al.*, Electron spin coherence exceeding seconds in high-purity silicon, Nat. Mater. **11**, 143 (2012).

[65] This preparation is possible by, for example, just waiting a long time that is longer than the thermal relaxation time, which is much longer than the coherence time.

[66] I. Chiorescu, Y. Nakamura, C. M. Harmans, and J. Mooij, Coherent quantum dynamics of a superconducting flux qubit, Science **299**, 1869 (2003).

[67] A. Lupaşcu, C. J. M. Verwijs, R. N. Schouten, C. J. P. M. Harmans, and J. E. Mooij, Nondestructive readout for a superconducting flux qubit, Phys. Rev. Lett. **93**, 177006 (2004).

[68] I. Chiorescu, P. Bertet, K. Semba, Y. Nakamura, C. Harmans, and J. Mooij, Coherent dynamics of a flux qubit coupled to a harmonic oscillator, Nature (London) **431**, 159 (2004).

[69] J. B. Majer, F. G. Paauw, A. C. J. Ter Haar, C. J. P. M. Harmans, and J. E. Mooij, Spectroscopy on two coupled superconducting flux qubits, Phys. Rev. Lett. **94**, 090501 (2005).

[70] F. G. Paauw, A. Fedorov, C. J. P. M. Harmans, and J. E. Mooij, Tuning the gap of a superconducting flux qubit, Phys. Rev. Lett. **102**, 090501 (2009).

[71] X. Zhu, A. Kemp, S. Saito, and K. Semba, Coherent operation of a gap-tunable flux qubit, Appl. Phys. Lett. **97**, 102503 (2010).

[72] N. Lambert, Y. Matsuzaki, K. Kakuyanagi, N. Ishida, S. Saito, and F. Nori, Superradiance with an ensemble of superconducting flux qubits, Phys. Rev. B **94**, 224510 (2016).

[73] K. Miyanishi, Y. Matsuzaki, H. Toida, K. Kakuyanagi, M. Negoro, M. Kitagawa, and S. Saito, Architecture to achieve nuclear magnetic resonance spectroscopy with a superconducting flux qubit, Phys. Rev. A **101**, 052303 (2020).

[74] R. P. Budoyo, K. Kakuyanagi, H. Toida, Y. Matsuzaki, and S. Saito, Electron spin resonance with up to 20 spin sensitivity measured using a superconducting flux qubit, Appl. Phys. Lett. **116**, 194001 (2020).

[75] J. Bylander, S. Gustavsson, F. Yan, F. Yoshihara, K. Harrabi, G. Fitch, D. G. Cory, Y. Nakamura, J.-S. Tsai, and W. D. Oliver, Noise spectroscopy through dynamical decoupling with a superconducting flux qubit, Nat. Phys. **7**, 565 (2011).

[76] A. Lupaşcu, S. Saito, T. Picot, P. de Groot, C. Harmans, and J. Mooij, Quantum non-demolition measurement of a superconducting two-level system, Nat. Phys. **3**, 119 (2007).

[77] Z. R. Lin, K. Inomata, W. D. Oliver, K. Koshino, Y. Nakamura, J. S. Tsai, and T. Yamamoto, Single-shot readout of a superconducting flux qubit with a flux-driven Josephson parametric amplifier, Appl. Phys. Lett. **103**, 132602 (2013).

[78] D. Marcos, M. Wubs, J. M. Taylor, R. Aguado, M. D. Lukin, and A. S. Sørensen, Coupling nitrogen-vacancy centers in diamond to superconducting flux qubits, Phys. Rev. Lett. **105**, 210501 (2010).

[79] J. Twamley and S. D. Barrett, Superconducting cavity bus for single nitrogen-vacancy defect centers in diamond, Phys. Rev. B **81**, 241202(R) (2010).

[80] X. Zhu, S. Saito, A. Kemp, K. Kakuyanagi, S.-i. Karimoto, H. Nakano, W. J. Munro, Y. Tokura, M. S. Everitt, K. Nemoto, *et al.*, Coherent coupling of a superconducting flux qubit to an electron spin ensemble in diamond, Nature (London) **478**, 221 (2011).

[81] S. Saito, X. Zhu, R. Amsüss, Y. Matsuzaki, K. Kakuyanagi, T. Shimo-Oka, N. Mizuochi, K. Nemoto, W. J. Munro, and K. Semba, Towards realizing a quantum memory for a superconducting qubit: Storage and retrieval of quantum states, Phys. Rev. Lett. **111**, 107008 (2013).

[82] X. Zhu, Y. Matsuzaki, R. Amsüss, K. Kakuyanagi, T. Shimo-Oka, N. Mizuochi, K. Nemoto, K. Semba, W. J. Munro, and S. Saito, Observation of dark states in a superconductor diamond quantum hybrid system, Nat. Commun. **5**, 3524 (2014).

[83] H. Nakazato, T. Takazawa, and K. Yuasa, Purification through Zeno-like measurements, Phys. Rev. Lett. **90**, 060401 (2003).

[84] J. K. Stockton, R. van Handel, and H. Mabuchi, Deterministic Dicke-state preparation with continuous measurement and control, Phys. Rev. A **70**, 022106 (2004).

[85] D. B. R. Dasari, S. Yang, A. Chakrabarti, A. Finkler, G. Kurizki, and J. Wrachtrup, Anti-Zeno purification of spin baths by quantum probe measurements, Nat. Commun. **13**, 7527 (2022).

[86] R. H. Dicke, Coherence in spontaneous radiation processes, Phys. Rev. **93**, 99 (1954).

[87] J. K. Stockton, J. M. Geremia, A. C. Doherty, and H. Mabuchi, Characterizing the entanglement of symmetric many-particle spin-1/2 systems, Phys. Rev. A **67**, 022112 (2003).

[88] N. Kiesel, W. Wieczorek, S. Krins, T. Bastin, H. Weinfurter, and E. Solano, Operational multipartite entanglement classes for symmetric photonic qubit states, Phys. Rev. A **81**, 032316 (2010).

[89] T. Benoist, M. Fraas, Y. Pautrat, and C. Pellegrini, Invariant measure for quantum trajectories, Probab. Theory Relat. Fields **174**, 307 (2019).

[90] K. Mochizuki and R. Hamazaki, Measurement-induced spectral transition, Phys. Rev. Lett. **134**, 010410 (2025).

[91] Note that we get $q = 1.995$, almost $q = 2$, when we numerically calculate the value of $C_{\rm cat}(\hat{S}_z, \hat{\rho}_{\rm PM})$ of a generalized cat state with $N = 63$, 127, and 1027 and perform a fitting, from which we expect $q \to 2$ with large N even with our scheme.

[92] S. Dengis, S. Wimberger, and P. Schlagheck, Multimode NOON-state generation with ultracold atoms via geodesic counterdiabatic driving, Phys. Rev. A **112**, 042610 (2025).

[93] M. Odelli, V. M. Stojanović, and A. Ruschhaupt, Spin squeezing in internal bosonic Josephson junctions via enhanced shortcuts to adiabaticity, Phys. Rev. Appl. **20**, 054038 (2023).

[94] M. Odelli, A. Ruschhaupt, and V. M. Stojanović, Twist-and-turn dynamics of spin squeezing in bosonic Josephson junctions: Enhanced shortcuts-to-adiabaticity approach, Phys. Rev. A **110**, 022610 (2024).

[95] S. L. Wu, W. Ma, X. L. Huang, and X. Yi, Shortcuts to adiabaticity for open quantum systems and a mixed-state inverse engineering scheme, Phys. Rev. Appl. **16**, 044028 (2021).

[96] M. Tatsuta, Y. Matsuzaki, H. Kuji, R. Hamazaki, and A. Shimizu, Dataset of "Characterization and generation of a standard-quantum-limit-beating cat-like state through repetitive measurements" [Data set], Zenodo (2026), doi:10.5281/zenodo.18168860.